Cell Reports

Article

Adamtsl3 mediates DCC signaling to selectively promote GABAergic synapse function

Graphical abstract

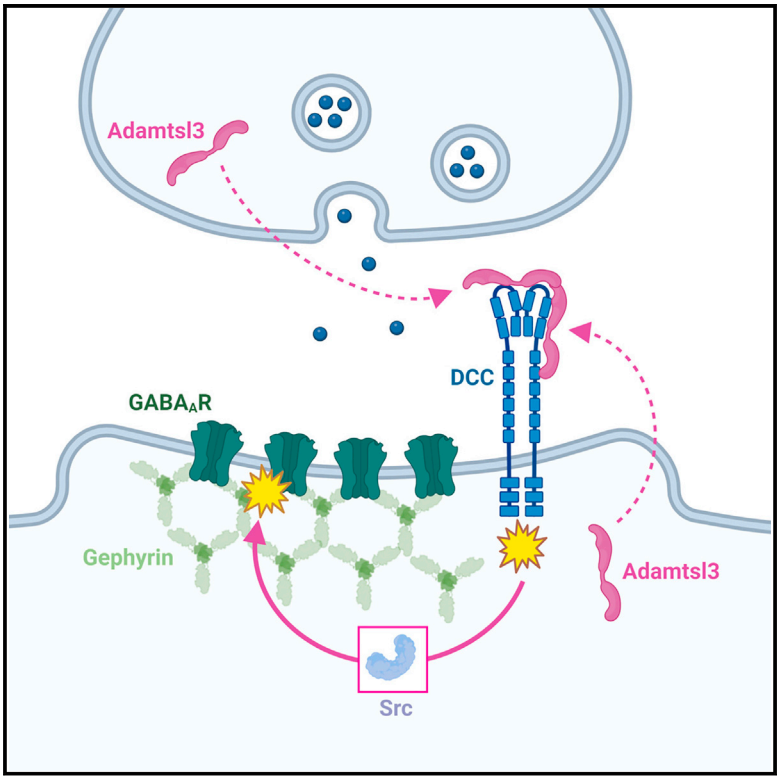

Authors

Teresa M.L. Cramer,
Berangere Pinan-Lucarre,
Anna Cavaccini, ..., Theofanis Karayannis,
Jean-Louis Bessereau,
Shiva K. Tyagarajan

Correspondence

shiva.tyagarajan@gmail.com

In brief

The secreted glycoprotein Ce-Punctin clusters neurotransmitter receptors at the *C. elegans* NMJ. Cramer et al. reveal that Ce-Punctin ortholog Adamtsl3 is a synaptic protein influencing synapse formation via the DCC receptor in the mouse brain. In the adult hippocampus, Adamtsl3-DCC signaling specializes toward GABAergic synapse function with behavioral consequences.

Highlights

- Adamtsl3 is widely expressed at hippocampal synapses
- Adamtsl3 is a ligand for DCC during synaptogenesis and in the mature brain
- Presynaptic and postsynaptic Adamtsl3 contribute toward GABAergic synapse maintenance via DCC
- Autocrine Adamtsl3-DCC signaling mediates plasticity adaptations at GABAergic postsynapse

Cramer et al., 2023, Cell Reports *42*, 112947
August 29, 2023
https://doi.org/10.1016/j.celrep.2023.112947

CellPress

Cell Reports

CellPress
OPEN ACCESS

Article

Adamtsl3 mediates DCC signaling to selectively promote GABAergic synapse function

Teresa M.L. Cramer,[1] Berangere Pinan-Lucarre,[3] Anna Cavaccini,[2] Angeliki Damilou,[2] Yuan-Chen Tsai,[1] Musadiq A. Bhat,[1] Patrizia Panzanelli,[4] Nicolas Rama,[5] Patrick Mehlen,[5] Dietmar Benke,[1] Theofanis Karayannis,[2] Jean-Louis Bessereau,[3] and Shiva K. Tyagarajan[1,6,*]

[1]University of Zurich, Institute of Pharmacology and Toxicology, Winterthurerstrasse 190, 8057 Zurich, Switzerland
[2]University of Zurich, Brain Research Institute, Winterthurerstrasse 190, 8057 Zurich, Switzerland
[3]University Claude Bernard Lyon 1, CNRS UMR 5284, INSERM U 1314, Melis, 69008 Lyon, France
[4]Department of Neuroscience Rita Levi Montalcini, University of Turin, Turin, Italy
[5]Centre de Recherche en Cancérologie de Lyon, INSERM U1052-CNRS UMR5286, Université de Lyon, Centre Léon Bérard, 69008 Lyon, France
[6]Lead contact
*Correspondence: shiva.tyagarajan@gmail.com
https://doi.org/10.1016/j.celrep.2023.112947

SUMMARY

The molecular code that controls synapse formation and maintenance *in vivo* has remained quite sparse. Here, we identify that the secreted protein Adamtsl3 functions as critical hippocampal synapse organizer acting through the transmembrane receptor DCC (deleted in colorectal cancer). Traditionally, DCC function has been associated with glutamatergic synaptogenesis and plasticity in response to Netrin-1 signaling. We demonstrate that early post-natal deletion of *Adamtsl3* in neurons impairs DCC protein expression, causing reduced density of both glutamatergic and GABAergic synapses. Adult deletion of *Adamtsl3* in either GABAergic or glutamatergic neurons does not interfere with DCC-Netrin-1 function at glutamatergic synapses but controls DCC signaling at GABAergic synapses. The Adamtsl3-DCC signaling unit is further essential for activity-dependent adaptations at GABAergic synapses, involving DCC phosphorylation and Src kinase activation. These findings might be particularly relevant for schizophrenia because genetic variants in *Adamtsl3* and *DCC* have been independently linked with schizophrenia in patients.

INTRODUCTION

Synapse organizers are important facilitators of *trans*-synaptic adhesion and assembly of presynapse and postsynapse during brain development and synapse maintenance in adulthood. Presynaptic Neurexin and postsynaptic Neuroligin (NLG) partners are examples of prototypical synapse organizers. Thousands of neurexin splice cassettes are differentially expressed within a typical neuron type.[1] Direct interaction not only occurs with NLG1 and NLG2 at excitatory and inhibitory synapses, respectively,[2] but with a range of signaling proteins (LRRTMs, latrophilins)[3] and $GABA_A$ (γ-aminobutyric acid type A) receptors[4] at the postsynaptic membrane. Hence a continuum of presynaptic and postsynaptic interactions is thought to contribute to the molecular logic of synaptic connections.[5]

Synapse organizers also play key roles during neural circuit assembly. Adhesion of the extracellular synapse organizer Netrin-1 to its cognate receptor DCC (Deleted in Colorectal Cancer) is necessary for attractive axon guidance and synaptogenesis during development.[6,7] In the adult brain, Netrin-1-DCC interaction activates Src kinase to induce NMDAR-dependent long-term potentiation (LTP), whereby influencing memory and learning.[8] In the nematode *Caenorhabditis elegans*, UNC-6 (Netrin-1 homolog) and UNC-40 (DCC homolog) facilitate synaptic vesicle clustering at NMJs (neuromuscular junctions) by organizing the actin cytoskeleton.[9,10] A genetic screen identified a presynaptically secreted glycoprotein Ce-Punctin in *C. elegans* that was shown to align acetylcholine and $GABA_A$ receptors at postsynaptic sites with neurotransmitter-specific release sites.[11] Subsequent studies uncovered that Ce-Punctin binds and activates postsynaptic UNC-40/DCC for $GABA_A$ receptor maintenance via the recruitment of FRM-3/FARP1-2 and LIN-2/CASK.[12] The mammalian orthologs of Ce-Punctin, Adamts-like 1 and Adamts-like 3, belong to a class of extracellular glycoproteins related to the ADAMTS (A Disintegrin and Metalloprotease with Thrombospondin repeat) proteases but are devoid of proteolytic activity.[13] Adamtsl1 and Adamtsl3 were discovered in the cDNA of the human placenta library.[14] Adamtsl1 is primarily expressed in human and mouse skeletal muscle, whereas Adamtsl3 shows widespread expression in the brain and has been identified as a candidate gene for schizophrenia.[14–16]

Although several intracellular signaling pathways have been shown to contribute to $GABA_A$ receptor clustering and inhibitory synapse plasticity,[17,18] little is known about extracellular organizers that dictate GABAergic synapse formation and/or maintenance. The role of mammalian Ce-Punctin orthologs, as well as

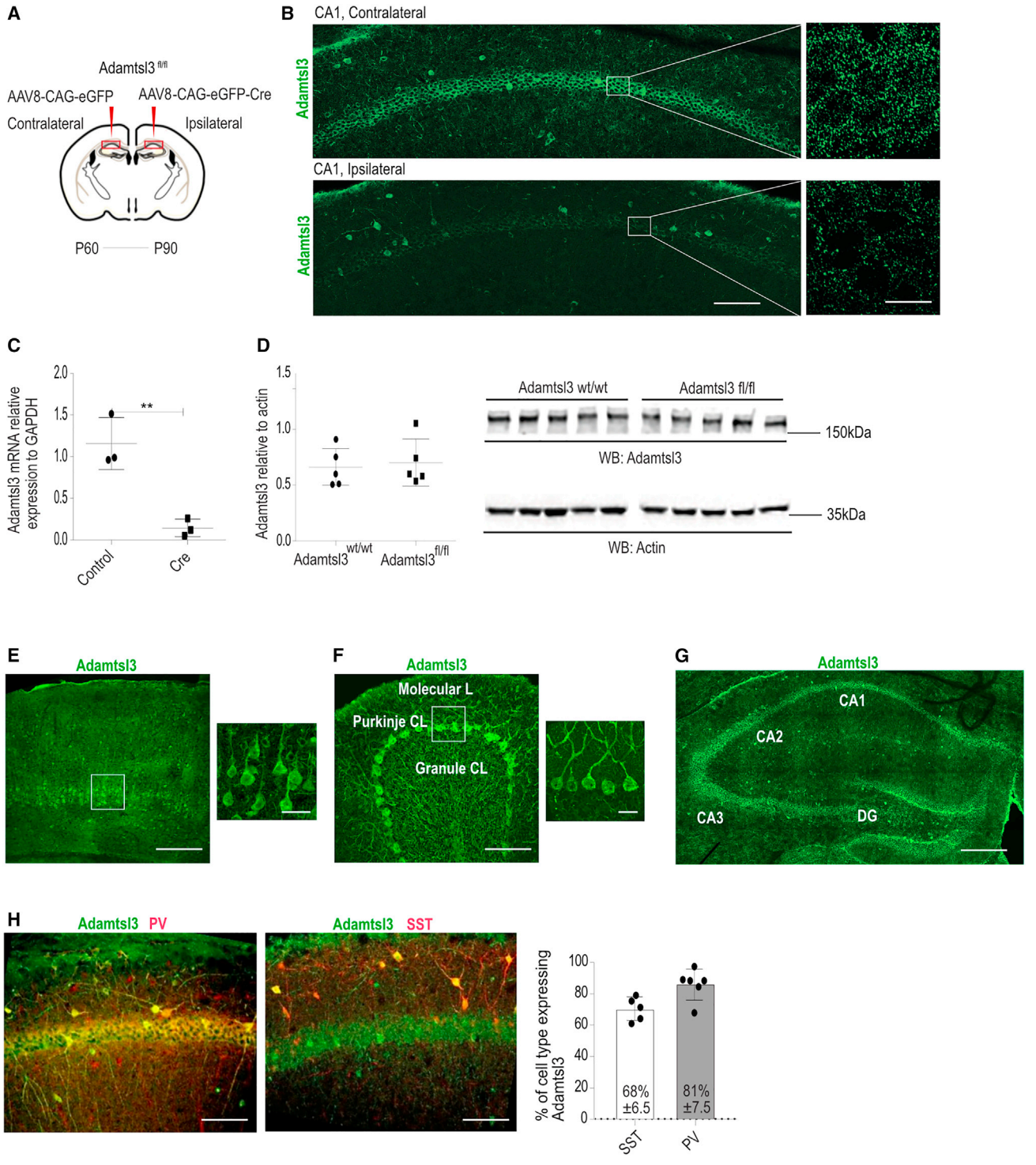

Figure 1. Adamtsl3 is widely expressed in the brain

(A) Illustration of *Adamtsl3*$^{flox/flox}$ mouse stereotaxically injected with AAV8-CAG-EGFP or AAV8-CAG-EGFP-Cre.

(B) Representative image of Adamtsl3 (green) after *Adamtsl3* deletion in CA1. Scale bar, 100 μm. Right panels are zoomed-in images of boxed areas in left panels. Scale bar, 5 μm.

(C) qRT-PCR analysis of *Adamtsl3* mRNA in AAV8-hSyn1-RFP- (control) or AAV8-hSyn1-RFP-Cre (Cre)-infected primary neuron cultures grown from P0–1 *Adamtsl3*$^{flox/flox}$ pups (n = 3 biological replicates).

(D) WB for Adamtsl3 in *Adamtsl3*$^{w/w}$ or *Adamtsl3*$^{flox/flox}$ forebrain lysates (n = 5).

(legend continued on next page)

the function of DCC at GABAergic synapses in the brain, have remained entirely uncharacterized. Here, we set out to characterize the function of Adamtsl3 in the mammalian brain. Using a combination of *in vitro* HEK293T-neuron co-culture and AAV8-Syn1-Cre to delete *Adamtsl3* in hippocampal neurons at birth, we uncover that Adamtsl3 functions in DCC-dependent assembly of GABAergic and glutamatergic synapses in early post-natal development. Using a combination of AAV6-CaMKII$\alpha^{ERT2\text{-}Cre}$ or AAV8-Dlx$^{ERT2\text{-}Cre}$ to delete *Adamtsl3* or *DCC* in pyramidal neurons or GABAergic interneurons, we report that Adamtsl3 functions upstream of DCC signaling for GABAergic synapse maintenance in the adult brain. We further provide evidence that Adamtsl3 signaling at the DCC receptor in the mature brain specifically influences GABAergic synapse integrity, whereas Netrin-1 signaling influences glutamatergic synapse integrity. In line with this, we demonstrate that Adamtsl3 functions in activity-dependent plasticity adaptations at GABAergic synapses via DCC and Src activation for hippocampal memory function. Together, our data identify an extracellular synapse organizer Adamtsl3 that signals via DCC at GABAergic synapses.

RESULTS

Adamtsl3 is widely expressed in the rodent brain

To understand the functional role of Adamtsl3 in the mammalian brain, we generated *Adamtsl3$^{flox/flox}$* mice in BL6 background by inserting *loxP* sites into exon 2 (Cyagen). *Adamtsl3$^{flox/flox}$* mice are fertile and give birth to litters in expected Mendelian ratios without abnormal phenotype. To validate our mouse line, we stereotaxically injected *Adamtsl3$^{flox/flox}$* mice at post-natal day (P) 60 with an adeno-associated virus (AAV) serotype 8 (AAV8) expressing Cre under the control of the CAG promoter (AAV8-CAG-Cre-EGFP) into the cornu Ammonis (CA1) hippocampal area. The contralateral hemisphere CA1 area was injected with AAV8-CAG-EGFP as control (Figure 1A). Using our homemade rabbit polyclonal antibody against Adamtsl3 N-terminal sequence (QTKMHLSPEKKEEN), we observed a significant reduction of Adamtsl3 in the ipsilateral (Cre-injected) CA1 area, but not in the contralateral area (Figure 1B). To further validate our Adamtsl3 antibody, we performed western blot (WB) analysis in conditioned media of HEK293T transfected with recombinant EGFP-Adamtsl3 and in primary neuron culture media. Recombinant Adamtsl3 was detected using an anti-GFP antibody at ~210 kDa in HEK293T media, and the Adamtsl3 antibody convincingly detected endogenous Adamtsl3 in conditioned primary neuron media at 14 days *in vitro* (DIV) (Figure S1A). Next, we cultured primary neurons from P0–1 *Adamtsl3$^{flox/flox}$* litters and infected them with either AAV8-hSyn1-RFP-Cre (Cre) or AAV8-hSyn1-RFP (control) at 4 DIV for Cre-dependent *Adamtsl3* gene deletion. At 14 DIV, we collected total cell RNA and performed quantitative reverse-transcription polymerase chain reaction (qRT-PCR) and found a significant reduction in *Adamtsl3* mRNA (Figure 1C). To confirm Adamtsl3 protein loss, we additionally performed immunohistochemical and WB analysis and found a significant loss of Adamtsl3 in Cre-expressing *Adamtsl3$^{flox/flox}$* neurons (Figures S1B–S1D). Lastly, to control for functional conservation of the gene locus during the generation of *Adamtsl3$^{flox/flox}$* mice, we analyzed for Adamtsl3 protein levels between *Adamtsl3$^{w/w}$* and *Adamtsl3$^{flox/flox}$* mice using WB and found no difference in Adamtsl3 expression (Figure 1D).

To understand the expression profile of Adamtsl3, we performed WB analysis using our validated Adamtsl3 antibody in lysates from the cortex, hippocampus, and cerebellum and found expression levels to be slightly increased in the cerebellum compared with the cortex and hippocampus (Figure S1E). Next, we determined the expression profile of *Adamtsl3* mRNA across different developmental time points. We used qRT-PCR analysis of cDNA libraries prepared from the cortex, hippocampus, and cerebellum of P5, P9, P15, and P30 BL6 mice (Figures S1F–S1H). *Adamtsl3* mRNA expression peaks first in the hippocampus at P5, followed by the cortex at P9, and then the cerebellum at P15. In the mature brain (P30), *Adamtsl3* mRNA expression across the cortex, cerebellum, and hippocampus decreases in comparison with earlier developmental time windows. Morphologically, we could localize Adamtsl3 across all cortical layers (Figure 1E), and we found it to be expressed within both pyramidal neurons and inhibitory neurons. In the cerebellum, Adamtsl3 labels the Purkinje cell soma and its dendritic branches extending into the molecular layer (Figure 1F). In the hippocampus, Adamtsl3 expression is uniform across CA1, CA2, and CA3 *Stratum pyramidale* and within interneurons in the *Stratum radiatum* and *oriens* (Figures 1G and 1H). Quantification confirmed Adamtsl3 expression within 81% of Parvalbumin (PV$^+$) and 68% of Somatostatin (SST$^+$) GABAergic interneurons (Figure 1H). Together, our data identify Adamtsl3 to be abundantly expressed within the mammalian brain.

Adamtsl3 is a synaptic protein regulating GABAergic and glutamatergic synapse number

To assess whether Adamtsl3 is enriched at synapses, we fractionated the rodent brain into biochemical subcompartments. Analysis of the synaptoneurosome fraction showed enrichment for Adamtsl3 protein along with $GABA_A$ receptor subunit α2, whereas the control nuclear fraction lacked Adamtsl3 (Figure 2A). Next, we investigated the proportion of excitatory and inhibitory hippocampal synapses that contain Adamtsl3. We co-stained for Adamstl3 along with presynaptic and postsynaptic markers for glutamatergic and GABAergic synapses in P90 BL6 mice (Figure 2B). We defined Adamtsl3 localization at synapses by points of spatial overlap (co-localization hereafter) between the signals generated by Adamtsl3 marker and presynaptic/postsynaptic marker. Based on the well-described subcellular distribution of glutamatergic and GABAergic synapses onto hippocampal CA1 pyramidal cells, we focused on the *S. pyramidale*

(E–G) Representative image showing Adamtsl3 (green) staining in the cortex (E; scale bars, 100 μm [left]; 20 μm [right, zoomed-in image of white box on left]), cerebellum (F; scale bars, 100 μm [left]; 20 μm [right, zoomed-in image of white box on left])), and hippocampus (G; scale bar, 200 μm).

(H) Representative image for Adamtsl3 (green) staining in the CA1 area within parvalbumin (PV; red) and somatostatin (SST; red) interneurons. Scale bars, 100 μm. Right panel: quantification of double-positive cells (n = 5–6; PV SD ±6.8; SST SD ±9.9%). Data are shown as mean ± SD. **p < 0.01 as determined by Student's two-tailed t test.

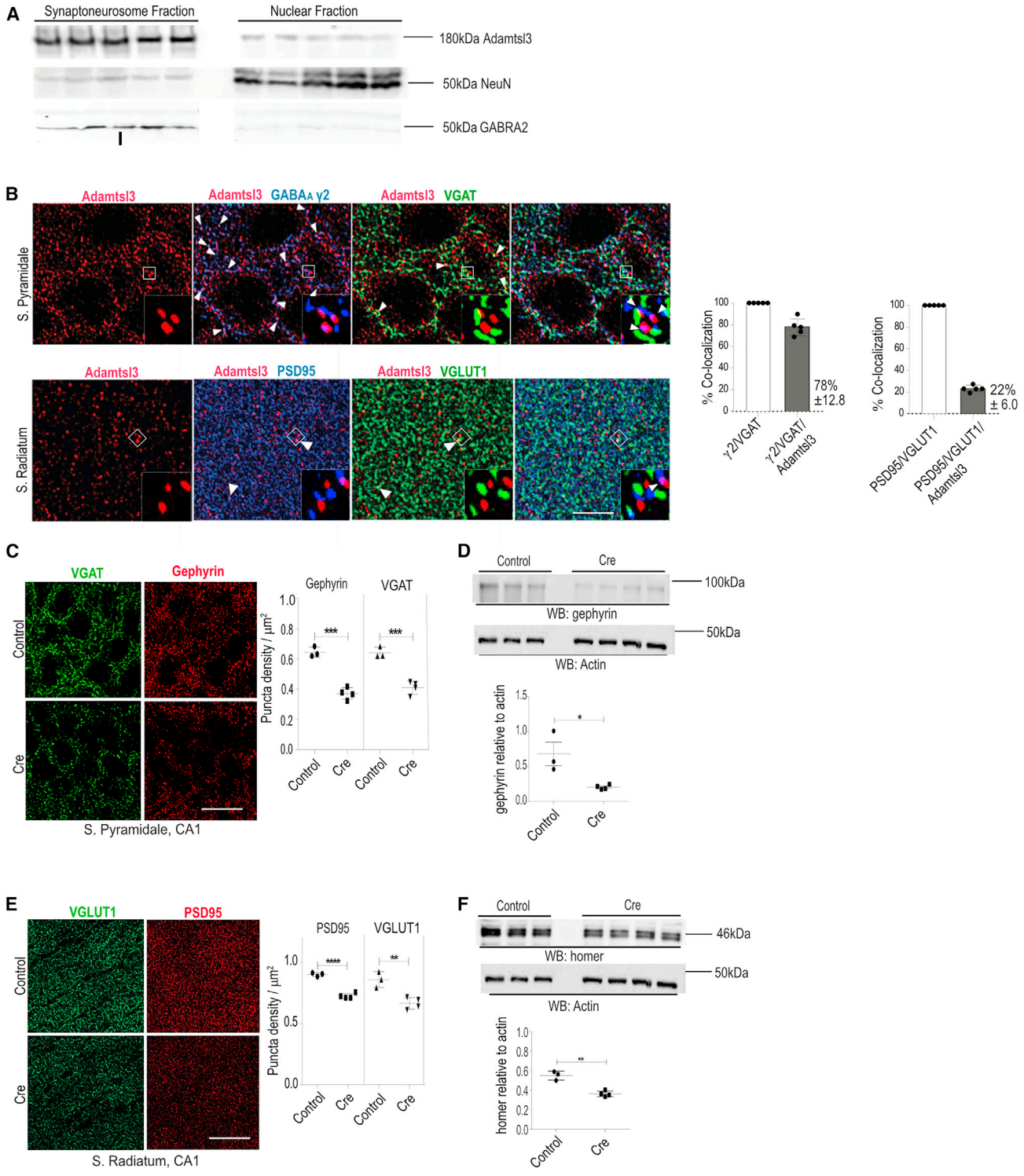

Figure 2. Adamtsl3 is a synaptic protein regulating GABAergic and glutamatergic synapse number

(A) Synaptoneurosome fraction showing enrichment for Adamtsl3 and GABRA2 (n = 5).

(B) Representative image of CA1 (top panel) *S. pyramidale* stained for Adamtsl3 (red), γ2 $GABA_AR$ subunit (blue), and VGAT (green) (n = 4; SD ±1.8%).; (bottom panel) *S. radiatum* stained for Adamtsl3 (red), PSD95 (blue), and VGlut1 (green) (n = 4; SD ±3.9%). Co-localization is shown using white arrowheads in zoom-in (white box).

(C) Left: representative images of CA1 *S. pyramidale* stained for VGAT (green) and gephyrin (red). Right: quantification of puncta densities. (n = 3–4).

(legend continued on next page)

for inhibitory synapses. Immunostaining for Adamtsl3 and GABAergic presynaptic and postsynaptic marker proteins showed that Adamtsl3 localizes with 78% of vesicular GABA transporter (VGAT) and γ2 subunit-containing $GABA_A$ receptors. In contrast, Adamtsl3 co-localizes with only 22% of vesicular glutamate transporter (VGlut1) and postsynaptic density protein 95 (PSD95) (Figure 2B) in the CA1 *S. radiatum*, where pyramidal cell dendrites are enriched for spines. This confirmed that Adamtsl3 is present at synapses and preferentially localized at GABAergic synapses.

To investigate the functional role of Adamtsl3 in the brain, we first tried to delete *Adamtsl3* during embryogenesis by generating the *Adamtsl3*$^{flox/flox}$/Nestin Cre$^{+/-}$ (CNS-specific Cre expression from embryonic day [E] 11) double-transgenic mouse line. We were unsuccessful in our attempts in generating this double-transgenic mouse, suggesting that Adamtsl3 is indispensable for embryonic development. Therefore, we investigated the role of Adamtsl3 in the post-natal brain by injecting the lateral ventricles of P0 *Adamtsl3*$^{flox/flox}$ pups with AAV8-hSyn1-RFP-Cre (Cre) or AAV8-hSyn1-RFP (control) virus (Figure S2A). Lateral ventricle P0 injection allowed for broad infectivity and expression within all hippocampal regions consistent with the published literature.[19] Using immunohistochemistry, we examined alterations to GABAergic synapse markers within CA1 *S. pyramidale*. Quantification for cluster density demonstrated a significant reduction in VGAT and gephyrin puncta in Cre-infected cells at P90 (Figure 2C). WB analysis of the hippocampal region for gephyrin protein expression upon control or Cre virus expression confirmed a significant reduction in the protein (Figure 2D). Immunohistochemical analysis for changes in glutamatergic synapse markers within *S. radiatum* showed a significant reduction in VGlut1 and PSD95 in Cre-infected cells at P90 (Figure 2E). WB analysis for another glutamatergic postsynaptic protein, Homer, also showed a significant reduction within the hippocampus of Cre-expressing mice compared with control animals (Figure 2F). Together, our data identify Adamtsl3 to be expressed at CA1 synapses and indicate a role for Adamtsl3 in both glutamatergic and GABAergic synapse formation and/or maintenance.

Adamtsl3 deletion in mature circuit impairs GABAergic neurotransmission

To evaluate the importance of Adamtsl3 in the adult brain, we utilized tamoxifen (TAM^+)-dependent Cre nuclear localization. We injected P0 *Adamtsl3*$^{flox/flox}$ pups intracranially with AAV8-hSyn1$^{ERT2\text{-}Cre}$ (Figure S2B). At P60, Cre expression was induced by injecting tamoxifen (TAM^+) for 5 consecutive days intraperitoneally (i.p.), to facilitate maximum Cre-dependent recombination.[20] Control mice from the same cohort did not receive TAM^+ injections, only vehicle (control). At P90, we analyzed for GABAergic synapse markers within CA1 *S. pyramidale* and observed a significant reduction of gephyrin but no change in VGAT in TAM^+ animals (Figure 3A). These results suggest that in the adult brain, Adamtsl3 function might be restricted to GABAergic postsynaptic maintenance and function.

Because Adamtsl3 is expressed within both pyramidal neurons and interneurons, we subsequently examined the effect of neuron-subtype-specific deletion of *Adamtsl3*. We injected P0 *Adamtsl3*$^{flox/flox}$ pups' lateral ventricles with AAV6-Calcium/calmodulin-dependent protein kinase type II subunit alpha (CaMKIIα)$^{ERT2\text{-}Cre}$ or AAV8-hDlx$^{ERT2\text{-}Cre}$ to ablate *Adamtsl3* either within pyramidal neurons or GABAergic interneurons, respectively (Figure S2B). At P60, Cre expression was induced by injecting TAM^+ for 5 consecutive days i.p., to facilitate maximum Cre-dependent recombination.[20] Control mice from the same cohort did not receive TAM^+ injections, only vehicle (control). At P90, we analyzed for GABAergic synapse markers within CA1 *S. pyramidale* of AAV6-CaMKII$\alpha^{ERT2\text{-}Cre}$-infected mice and found a significant reduction in gephyrin marker but no change in VGAT in TAM^+ mice (Figure 3B). Similarly, we analyzed for changes in GABAergic synapse markers in mice injected with AAV8-hDlx$^{ERT2\text{-}Cre}$. Immunohistochemical analysis and quantification also showed reduced gephyrin clusters but no change in VGAT clusters upon *Adamtsl3* deletion from GABAergic interneurons (Figure 3C). WB analysis for total gephyrin protein in AAV6-CaMKII$\alpha^{ERT2\text{-}Cre}$- or AAV8-hDlx$^{ERT2\text{-}Cre}$-injected brains (control/TAM^+) confirmed reduced gephyrin levels within the hippocampus after TAM^+-induced Cre nuclear localization (Figures 3D and 3E). Our data identify that Adamtsl3 within either pyramidal cells or GABAergic interneurons in the adult brain specifically impacts the postsynaptic apparatus through gephyrin loss at CA1 GABAergic synapses.

The scaffolding protein gephyrin is functionally associated with $GABA_A$ receptors localized at synaptic sites, which mediate most inhibitory synaptic transmission.[21] Hence we wondered whether reduced gephyrin clustering reflected a loss of synaptic $GABA_A$ receptors. To test this, we assessed the expression of α2 $GABA_A$ receptors subunit in *Adamtsl3*$^{flox/flox}$ pups intracranially injected with AAV8-hSyn1$^{ERT2\text{-}Cre}$. The α2 subunit is among the most prevalent subunits present in CA1 synaptic $GABA_A$ receptors.[22] Compared with control animals, we observed a significant reduction in the α2 subunit within the CA1 *S. pyramidale* of TAM^+ AAV8-hSyn1$^{ERT2\text{-}Cre}$-injected mice at P90 (Figure S3C), indicating that gephyrin reduction reflects a loss of synaptic $GABA_A$ receptors.

Because both pyramidal neuron- and interneuron-specific deletion of *Adamtsl3* reduced gephyrin clustering, we subsequently examined their functional consequence to GABAergic inhibition. We injected P0 *Adamtsl3*$^{flox/flox}$ mice with AAV6-CaMKII$\alpha^{ERT2\text{-}Cre}$ or AAV8-Dlx$^{ERT2\text{-}Cre}$ and induced TAM^+-dependent Cre nuclear localization at P60. At P90, we recorded miniature inhibitory postsynaptic currents (mIPSCs) from CA1 pyramidal neurons in the presence of tetrodotoxin (TTX), cyanquixaline (CNQX), and (2R)-2-amino-5-phosphonopentanoic acid (AP-5) (Figures 3F and 3G). As expected, TAM^+ neurons expressing AAV6-CaMKII$\alpha^{ERT2\text{-}Cre}$ displayed reduced mIPSC

(D) WB for gephyrin after *Adamtsl3* deletion (n = 3–4).
(E) Left: representative images of CA1 *S. radiatum* stained for VGlut1 (green) and PSD95 (red). Right: quantification of puncta densities (n = 3–4).
(F) WB for homer after *Adamtsl3* deletion (n = 3–4). Scale bar, 5 μm.
Data are shown as mean ± SD. **p < 0.01, ***p < 0.005, ****p < 0.0001, as determined by Student's two-tailed t test.

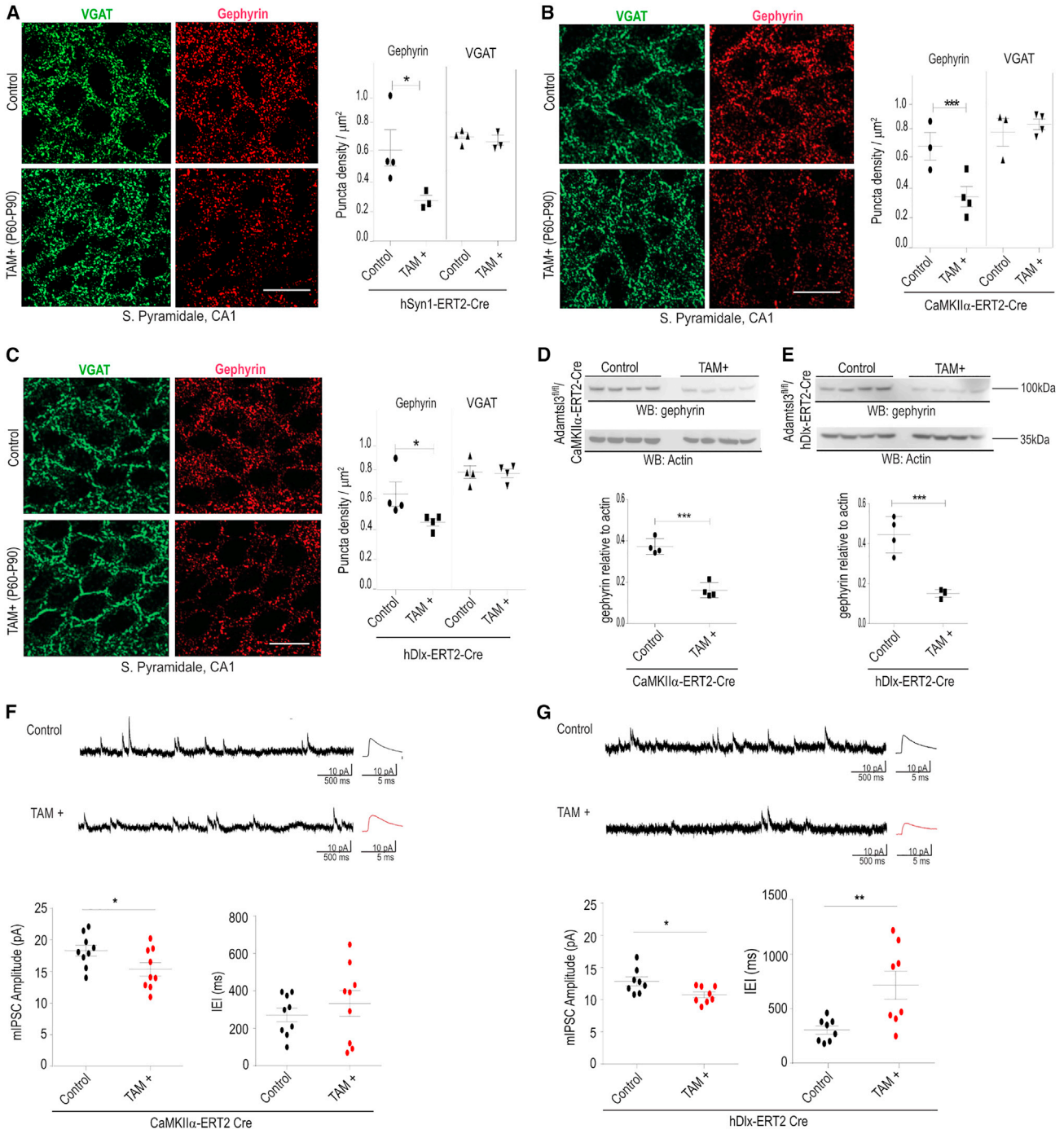

Figure 3. Neuron-specific deletion of Adamtsl3 causes structural and functional defects at GABAergic synapses

(A) Left: representative images of CA1 *S. pyramidale* stained for VGAT (green) and gephyrin (red) in AAV8-hSyn1$^{ERT2\text{-}Cre}$ (control/TAM^{+}) animals. Right: quantification of puncta densities (n = 3–4).

(B) Left: representative images of CA1 *S. pyramidale* stained for VGAT (green) and gephyrin (red) in AAV6-CaMKIIα$^{ERT2\text{-}Cre}$ (control/TAM^{+}) animals. Right: quantification of puncta densities (n = 3–4).

(C) Left: representative images of CA1 *S. pyramidale* stained for VGAT (green) and gephyrin (red) in AAV8-hDlx$^{ERT2\text{-}Cre}$ (control/TAM^{+}) animals. Right: quantification of puncta densities (n = 3–4). Scale bar, 5 µm.

(D) WB of hippocampal lysates from AAV6-CaMKIIα$^{ERT2\text{-}Cre}$ (control/TAM^{+}) animals for gephyrin (n = 4).

(E) WB of hippocampal lysates from AAV8-hDlx$^{ERT2\text{-}Cre}$ (control/TAM^{+}) animals for gephyrin (n = 4). Data are shown as mean ± SD.

(legend continued on next page)

amplitude (15.36 ± 1.07 pA) compared with controls (18.8 ± 0.86 pA; Figure 3F). The mIPSC inter-event interval (IEI) was unaltered in AAV6-CaMKIIα$^{ERT2\text{-}Cre}$-expressing neurons (TAM$^+$ vs. control: 332.9 ± 68.85 ms vs. 271.3 ± 36.36 ms; Figure 3F). Similarly, TAM$^+$ neurons expressing AAV8-Dlx$^{ERT2\text{-}Cre}$ demonstrated reduced mIPSC amplitude (10.74 ± 0.45 pA) compared with controls (12.84 ± 0.68 pA; Figure 3G). Although we did not detect morphological changes in the number of VGAT-positive terminals in *Adamtsl3$^{flox/flox}$* mice injected with AAV8-Dlx$^{ERT2\text{-}Cre}$, we did detect a significant increase in mIPSC IEIs (TAM$^+$ vs. control: 715.2 ± 129.7 ms vs. 304.1 ± 36.68 ms; Figure 3G). These results suggest that our immunohistochemical analysis was not sensitive enough to detect differences in VGAT marker density or that observed IEI changes involve differences in synaptic vesicle mobilization/fusion. Importantly, we did not detect any changes in miniature excitatory postsynaptic currents (mEPSCs) in either AAV6-CaMKIIα$^{ERT2\text{-}Cre}$-expressing or AAV8-Dlx$^{ERT2\text{-}Cre}$ neurons (Figures S2D and S2E). These results confirm that Adamtsl3 maintains GABAergic neurotransmission in the adult brain.

Adamtsl3 influences DCC receptor function at GABAergic synapses

Genetic deletion of *Adamtsl3* decreases GABAergic synapse markers at CA1 pyramidal cell somata, indicating that Adamtsl3 influences inhibitory synapse formation during development and synapse maintenance in adulthood. To test whether Adamtsl3 is a synaptogenic molecule, we used a neuron-HEK293T co-culture assay that has previously been described to successfully identify synaptogenic molecules.[23] In brief, we cultured primary hippocampal neurons from P0–1 *Adamtsl3$^{flox/flox}$* litters and infected them at 4 DIV with either AAV8-hSyn1-RFP-Cre (Cre) or AAV8-hSyn1-RFP (control). At 7 DIV, we seeded HEK293T cells transfected with plasmid encoding N-Cadherin, NLG1, NLG2, or DCC on top. At 9 DIV, we examined for VGAT- or VGlut1-positive synapse recruitment (Figure S3A).

HEK293T cells transfected with N-Cadherin served as adhesive, non-synaptogenic control. Compared to N-Cadherin, control neurons formed VGAT positive terminals as efficiently as Cre-infected neurons at NLG2, a postsynaptic cell adhesion molecule implicated in inhibitory synapse formation (Figure S3B). Similarly, we found Cre-infected neurons to form VGlut1 positive terminals as efficiently as control neurons at NLG1, a postsynaptic cell adhesion molecule implicated in excitatory synapse formation (Figure S3C). These results indicate that NLG1 and 2 function at glutamatergic and GABAergic synapses is independent of Adamtsl3. In *C. elegans* it has been reported that Ce-Punctin acts through the UNC-40/DCC receptor to impact NMJs.[11] DCC has previously been reported to facilitate the induction of glutamatergic presynaptic structures *in vitro*.[24] Compared with N-Cadherin, we found DCC to efficiently recruit VGlut1 and VGAT positive terminals in control neurons but not in Cre-infected neurons (Figures S3B and S3C). These results identify a role for Adamtsl3 in DCC-dependent synapse formation of both glutamatergic and GABAergic synapses *in vitro*. A role for Adamtsl3 in synapse formation is consistent with our earlier observations where P0 deletion of *Adamtsl3* reduces glutamatergic and GABAergic synapse density *in vivo* (Figures 2C and 2E).

DCC receptor function at glutamatergic synapses has been described in the literature, but little is known about DCC expression or function at inhibitory synapses. We first evaluated DCC enrichment in synaptoneurosomes using WB, confirming the report by Horn et al.[8] that DCC is enriched at synaptic sites (Figure S3D). Next, using immunohistochemistry we assessed DCC co-localization with glutamatergic and GABAergic synapse markers. Quantification showed that 61% of PSD95 and VGlut1-containing synapses also co-label for DCC in the *S. radiatum* (Figure S3E), which is consistent with previous reports describing DCC co-localization at glutamatergic synapses in primary neurons.[25] Co-localization with inhibitory synapse markers ($GABA_A$ receptor γ2 subunit and VGAT) in the *S. pyramidale* showed 96% overlap (Figure S3E). These findings are consistent with proteomic analysis showing DCC localization at inhibitory synapses.[26]

To better understand the relationship between Adamtsl3 and DCC *in vivo*, we examined the expression of DCC in *Adamtsl3$^{flox/flox}$* mice infected with either AAV8-hSyn1-RFP-Cre (Cre) or AAV8-hSyn1-RFP (control) at P0. Immunohistochemical analysis at P90 showed reduced DCC puncta in the CA1 *S. pyramidale* of Cre-expressing mice (Figure 4A). We next assessed how *Adamtsl3* deletion in adult neurons influenced DCC expression *in vivo*. Similar to *Adamtsl3* deletion at birth, immunohistochemical analysis for DCC expression in the CA1 *S. pyramidale* of TAM$^+$ AAV8-hSyn1$^{ERT2\text{-}Cre}$-injected mice showed a reduction in DCC expression compared to controls (Figure 4B). Immunohistochemical analysis in the CA1 *S. pyramidale* of TAM$^+$ AAV6-CaMKIIα$^{ERT2\text{-}Cre}$ injected mice showed no change in DCC expression compared to controls (Figure 4C), while we found a significant reduction in TAM$^+$ mice injected with AAV8-hDlx$^{ERT2\text{-}Cre}$ (Figure 4D). DCC co-localization with PSD95 in *S. radiatum* of AAV8-hDlx$^{ERT2\text{-}Cre}$ expressing mice remained unchanged, indicating that DCC loss is restricted to GABAergic synapses (Figure S3F). Combined, these results indicate that Adamtsl3 from interneurons localizes DCC at CA1 GABAergic synapses.

If Adamtsl3 is a cognate DCC receptor ligand, then it should bind the DCC receptor and activate its downstream signal transduction pathway(s). To test for biochemical interaction between the two proteins, we immunoprecipitated (IP) EGFP-Adamtsl3 from transfected HEK293T media. Then, we incubated immobilized EGFP-Adamtsl3 with HEK293T lysate containing overexpressed myc-DCC. WB for DCC confirmed biochemical interaction between EGFP-Adamtsl3 and myc-DCC (Figure 4E). To confirm this finding, we evaluated the interaction between endogenous Adamtsl3 and myc-DCC using *in situ* proximity

(F) mIPSC representative traces in AAV6-CaMKIIα$^{ERT2\text{-}Cre}$ (control/TAM$^+$) animals, n = 9 cells; (bottom panel) mIPSC amplitude Tam$^+$ vs. controls and mIPSC inter-event-intervals TAM$^+$ vs. controls.

(G) mIPSC representative traces in AAV8-hDlx$^{ERT2\text{-}Cre}$ (control/TAM$^+$) animals, n = 9 cells; (bottom panel) mIPSC amplitude TAM$^+$ vs. controls and mIPSC inter-event-intervals Tam$^+$ vs. control.

Data are shown as mean ± SEM. *p < 0.05, **p < 0.01, ***p < 0.005, as determined by Student's two-tailed t test.

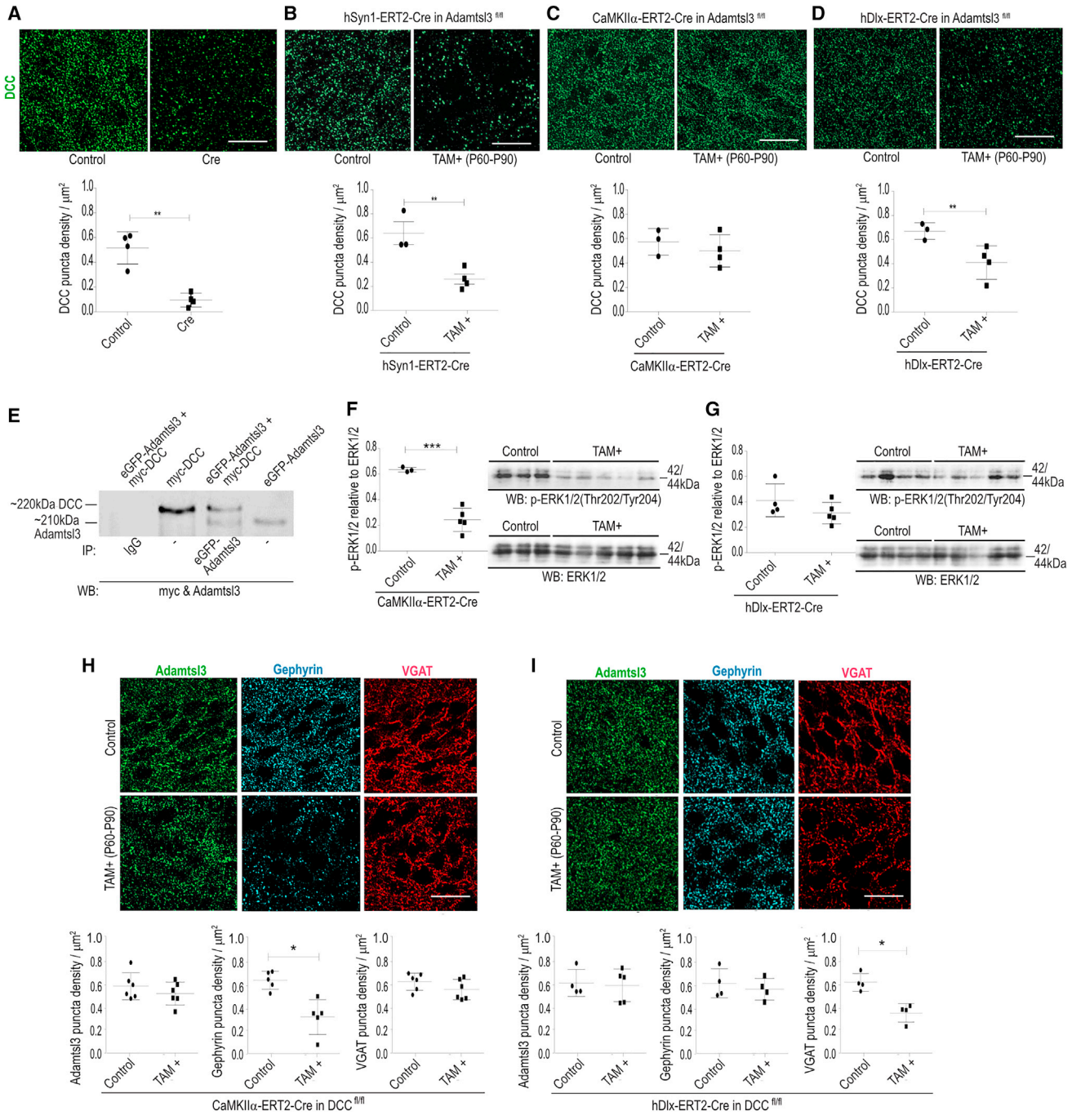

Figure 4. Adamtsl3 controls the synaptic localization of DCC, which is required for the maintenance of GABAergic synapses

(A) Representative images of CA1 *S. pyramidale* stained for DCC (green) in *Adamtsl3*$^{flox/flox}$ mice infected with AAV8-hSyn1-RFP-Cre (cre) or AAV8-hSyn1-RFP (control) (n = 4).

(B) CA1 *S. pyramidale* stained for DCC (green) in AAV8-hSyn1$^{ERT2\text{-}Cre}$ (control/TAM^{+})-infected mice (n = 3–4).

(C) CA1 *S. pyramidale* stained for DCC (green) in AAV6-CaMKIIα$^{ERT2\text{-}Cre}$ (control/TAM^{+})-infected mice (n = 3–4).

(D) CA1 *S. pyramidale* stained for DCC (green) in AAV8-hDlx$^{ERT2\text{-}Cre}$ (control/TAM^{+})-infected mice (n = 3–4).

(E) IP for EGFP-Adamtsl3 followed by WB for Adamtsl3 and myc-DCC.

(F and G) WB analysis of ERK1/2 and pERK1/2 in P90 *Adamtsl3*$^{flox/flox}$ hippocampal lysates after neuron-specific *Adamtsl3* deletion (n = 4–6).

(H) Top: representative images of *DCC*$^{flox/flox}$ CA1 neurons infected with AAV6-CaMKIIα$^{ERT2\text{-}Cre}$ (TAM^{+}/control) stained for Adamtsl3 (green), gephyrin (blue), and VGAT (red). Bottom: quantification of puncta densities (n = 5–6).

(legend continued on next page)

ligation assay (PLA) in primary hippocampal neurons. Using myc-tag and homemade Adamtsl3 antibody, we found few background signals in untransfected control neurons but a strong PLA signal in myc-DCC-transfected neurons (Figure S3G). Combined, our results demonstrate a biochemical interaction between Adamtsl3 and DCC.

To assess the activation of the signaling pathway(s) downstream of DCC, we performed WB analysis for mitogen activated kinase 1/2 (ERK1/2), a major downstream signaling kinase phosphorylated upon DCC activation.[27] We injected P0 *Adamtsl3*$^{flox/flox}$ pups' lateral ventricles with either AAV6-CaMKII$\alpha^{ERT2\text{-}Cre}$ or AAV8-hDlx$^{ERT2\text{-}Cre}$ and induced Cre expression at P60 with TAM^{+} (i.p.) injections. At P90, we performed WB analysis for ERK1/2 and its activated form pERK1/2 (phosphorylated at Thr202/Tyr204). Relative to total ERK1/2, pERK1/2 was significantly reduced in TAM^{+} *Adamtsl3*$^{flox/flox}$ mice injected with AAV6-CaMKII$\alpha^{ERT2\text{-}Cre}$ (Figure 4F). In contrast, (TAM^{+}/control) *Adamtsl3*$^{flox/flox}$ mice injected with AAV8-hDlx$^{ERT2\text{-}Cre}$ showed no difference in pERK1/2 levels relative to total ERK1/2 (Figure 4G). Combined, these findings give credence to the idea that Adamtsl3 is a ligand of DCC at synaptic sites. Further, our findings suggest specific presynaptic and postsynaptic contributions of Adamtsl3 to DCC receptor function at mature GABAergic synapses in CA1: whereas Adamtsl3 expression in interneurons localizes/stabilizes DCC at GABAergic sites, Adamtsl3 in pyramidal cells functions as an autocrine signaling molecule required for DCC receptor activation.

DCC loss impairs GABAergic synapses

DCC receptor has been localized to excitatory presynaptic and postsynaptic sites.[28] Although our results confirm DCC localization at GABAergic synapses, they do not clarify DCC expression and function at presynaptic and/or postsynaptic sites. To test the compartment-specific relevance of DCC at GABAergic synapses, we utilized *DCC*$^{flox/flox}$ mice and injected P0 pups' lateral ventricles with AAV6-CaMKII$\alpha^{ERT2\text{-}Cre}$ or AAV8-hDlx$^{ERT2\text{-}Cre}$ (Figure S4A). Cre recombination was induced at P60 using TAM^{+} (i.p.), and neuron-specific Cre expression was confirmed at P90. Immunohistochemical analysis within the CA1 *S. pyramidale* demonstrated DCC loss in both TAM^{+} CaMKIIα-$^{ERT2\text{-}Cre}$ and hDlx-$^{ERT2\text{-}Cre}$ mice compared with controls (Figure S4B). In line with the published literature on DCC at excitatory synapses, we demonstrate DCC receptor localization at both presynaptic and postsynaptic sites at CA1 GABAergic synapses.

Next, we looked for changes in Adamtsl3, gephyrin, and VGAT in CaMKII$\alpha^{ERT2\text{-}Cre}$-injected mice. Within the CA1 *S. pyramidale*, we found a significant reduction of gephyrin clusters in TAM^{+} mice but no change in VGAT (Figure 4H), indicating that DCC receptor expression in pyramidal cells is specifically required to maintain the GABAergic postsynaptic compartment. In TAM^{+} AAV8-hDlx$^{ERT2\text{-}Cre}$-injected mice, analysis for gephyrin and VGAT puncta showed a significant loss of VGAT puncta, whereas gephyrin and Adamtsl3 puncta were unaffected (Figure 4I), indicating that presynaptic DCC receptor facilitates the maintenance of GABAergic terminals onto CA1 pyramidal neurons. These findings are in line with reports of reduced presynaptic vesicle dynamics following glutamatergic presynaptic *DCC* deletion and weaker excitatory postsynaptic activity following postsynaptic *DCC* deletion.[29] Importantly, Adamtsl3 expression was not changed after *DCC* deletion from presynaptic or postsynaptic neurons (Figures 4H and 4I). Although the precise role of Adamtsl3 at presynaptic terminals requires further investigation, our results indicate that both presynaptic and postsynaptic Adamtsl3 function upstream of DCC expressed in pyramidal cells for the maintenance of GABAergic postsynapses.

Adamtsl3 activates the DCC receptor and its downstream Src effector

Our previous results have indicated that postsynaptic Adamtsl3 functions as an autocrine signaling molecule activating the DCC receptor at GABAergic postsynaptic sites. To understand the physiological relevance of Adamtsl3-DCC signaling, we induced inhibitory LTP (iLTP) using mild and brief NMDA receptor activation.[30] We prepared primary hippocampal cultures from P0–1 *Adamtsl3*$^{flox/flox}$ litters and infected them with either AAV8-hSyn1-RFP-Cre (Cre) or AAV8-hSyn1-RFP (control) at 4 DIV to delete *Adamtsl3*. At 14 DIV, we induced iLTP and measured for changes in pDCC (phosphorylated at Tyr1418) using WB at 60 min post-iLTP. We found a significant increase in pDCC compared with total DCC levels in control neurons after iLTP (Figure 5A). In contrast, we did not detect any change in pDCC levels after iLTP induction in Cre-infected neurons (Figure 5B).

Next, we quantified Adamtsl3 and gephyrin clusters along proximal dendrites and found a significant increase in their cluster densities at 60 min following iLTP induction (Figure 5C). Consistent with the pDCC data, neurons lacking Adamtsl3 did not show an increase in gephyrin cluster density (Figure 5D).

To confirm the specificity of Adamtsl3 toward GABAergic synapses, we induced chemical LTP (cLTP) at glutamatergic synapses in hippocampal cultures from P0–1 *Adamtsl3*$^{flox/flox}$ litters.[31] At 4 DIV, we infected *Adamtsl3*$^{flox/flox}$ neurons with either AAV8-hSyn1-RFP-Cre (Cre) or AAV8-hSyn1-RFP (control) and induced cLTP at 14 DIV. At 40 min after cLTP induction, we quantified pan-GluA1 and PSD95 clusters and found that expression of Adamtsl3 has no impact on their cluster densities (Figures 5E and 5F). These results confirm that Adamtsl3 specifically contributes to GABAergic synapse plasticity via DCC phosphorylation.

DCC phosphorylation has been reported to induce Src kinase activation, which directly impinges on $GABA_A$ receptor function through phosphorylation at γ2 subunit Tyr365/367, resulting in increased GABA currents.[32,33] To assess whether this molecular pathway is activated downstream of Adamtsl3 and DCC signaling, we performed WB analysis for pSrc (phosphorylated at Tyr416) in control *Adamtsl3*$^{flox/flox}$ hippocampal culture lysates collected 60 min post-iLTP. We found a significant

(I) Top: representative images of *DCC*$^{flox/flox}$ CA1 neurons infected with AAV8-hDlx$^{ERT2\text{-}Cre}$ (TAM^{+}/control) and stained for Adamtsl3 (green), gephyrin (blue), and VGAT (red). Bottom: quantification of puncta densities (n = 3–6). Scale bar, 5 μm.
Data are shown as mean ± SD. *p < 0.05, **p < 0.01, as determined by Student's two-tailed t test.

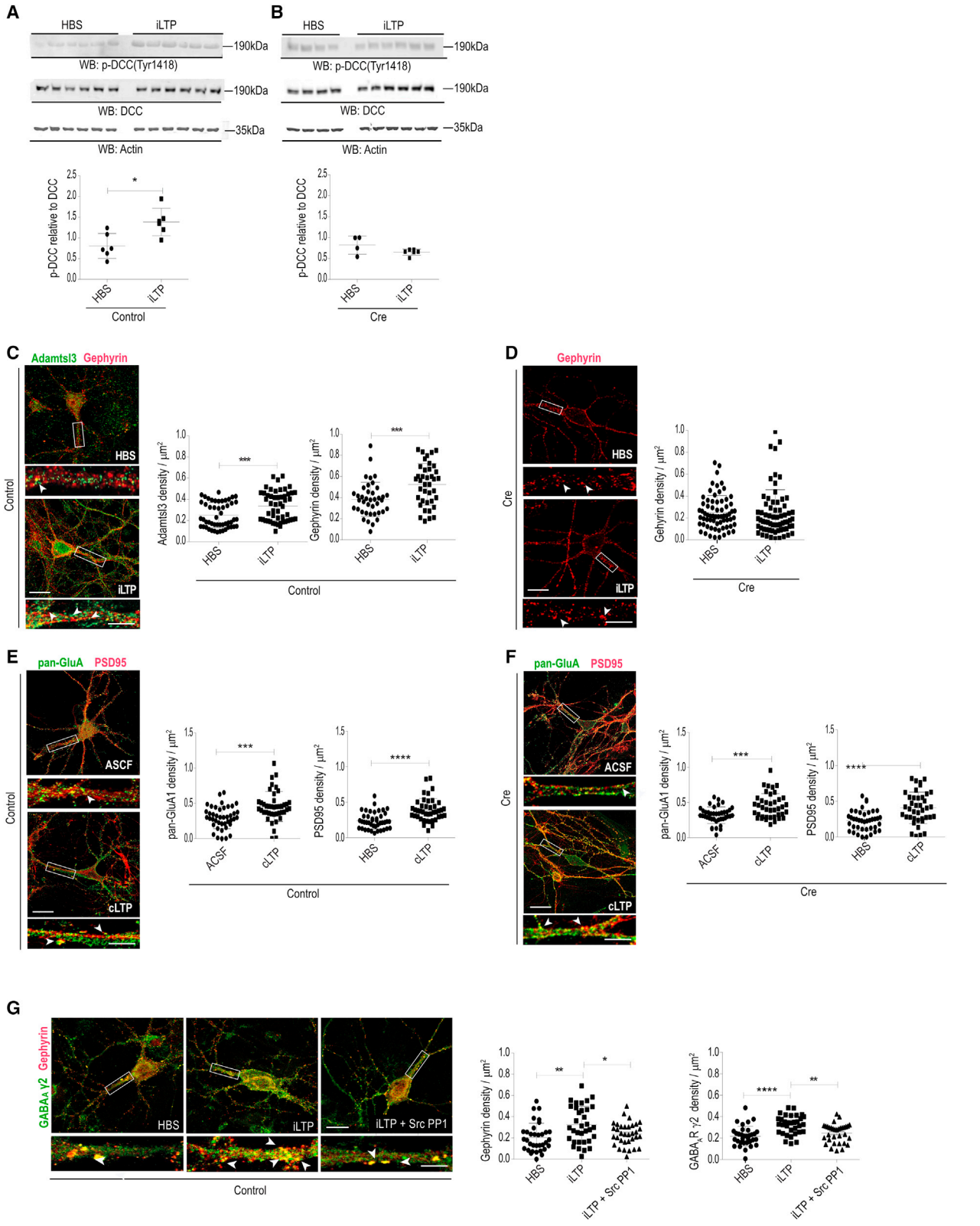

(legend on next page)

increase in pSrc compared with total Src levels at 60 min post-iLTP (Figure S5A). In contrast, Cre-infected cultures did not show an increase in pSrc at 60 min post-iLTP (Figure S5B). Quantification of γ2 $GABA_A$ receptor cluster density at 60 min following iLTP induction showed a significant increase in control-infected neurons (Figure 5G). Consistent with the pSrc data, neurons lacking Adamtsl3 did not show an increase in γ2 $GABA_A$ receptor cluster density (Figure S5C). As further validation, we pharmacologically blocked Src kinase using the inhibitor PP1 before iLTP induction in control neurons. We found that blocking Src kinase prevents an increase in GABAergic synapse marker density at 60 min post-iLTP (Figure 5G). Taken together, our results identify that Adamtsl3 signals via DCC and Src kinase to facilitate plasticity changes at GABAergic synapses.

Netrin-1 selectively regulates glutamatergic synapse maintenance

Our results so far suggest that Adamtsl3 is a ligand of DCC at GABAergic synapses in the adult brain. The cognate ligand for DCC, Netrin-1, has been reported to influence the DCC receptor at excitatory synapses with consequences for synapse function. To understand the relevance of Netrin-1 for inhibitory synapse maintenance, we set out to silence *Netrin-1* mRNA in the adult rodent brain. To ablate the *Netrin-1* gene product, we generated an AAV (in collaboration with viral vector core, University of Zurich, ETH Zurich (UZH/ETHZ) encoding a microRNA (miRNA)-embedded shRNA targeting *Netrin-1* in all neuronal cells (AAV8-Syn1-shRNA-NTN1). Primary neuron cultures grown from P0–1 BL6 litters were infected with AAV8-Syn1-shRNA-NTN1 (shNetrin1) or AAV8-hSyn1-shRNA-scramble (shControl) at 4 DIV to assess *Netrin-1* mRNA expression. At 14 DIV, RT-PCR indicated a significant loss of *Netrin-1* mRNA (Figure S6A), validating our shRNA gene-silencing approach.

Next, we stereotaxically injected the hippocampus of P60 BL6 mice with shNetrin-1 to knock down *Netrin-1* mRNA and the contralateral hippocampus with shControl (Figure S6B). Compared with the contralateral side, morphological analysis of DCC and PSD95 in the *S. radiatum* showed a significant reduction at P90 (Figure S6C). In contrast, analysis for DCC and gephyrin in the pyramidal cell layer did not show any reduction (Figure S6D). Adamtsl3 expression was further unchanged (Figure S6E). These findings indicate that Netrin-1 regulates glutamatergic synapse maintenance, whereas Adamtsl3 facilitates GABAergic synapse maintenance. Combined, our data identify Adamtsl3 as a ligand of DCC that specifically functions at GABAergic synapses in the adult brain.

Adamtsl3 is required for hippocampal-dependent memory

Our data identify an important role for Adamtsl3 and DCC at GABAergic synapses within the hippocampus. Because DCC has been implicated in learning and memory,[8,34] we investigated the impact of *Adamtsl3* deletion in the memory-related object displacement test (ODT) (Figure 6A). We injected P0 *Adamtsl3*$^{flox/flox}$ pups with either AAV8-hSyn1-RFP-Cre (Cre) or AAV8-hSyn1-RFP (control) to delete *Adamtsl3* early in post-natal brain development. At P90–105, we found control-injected mice spend significantly more time exploring the displaced object compared with Cre-injected animals (Figure S7A). To test the effect of *Adamtsl3* deletion in the adult brain, we injected P0 *Adamtsl3*$^{flox/flox}$ pups with either AAV6-CaMKIIα$^{ERT2\text{-}Cre}$ or AAV8-hDlx$^{ERT2\text{-}Cre}$ and induced Cre-dependent recombination at P60. At P90–105, we found both TAM$^+$ AAV6-CaMKIIα$^{ERT2\text{-}Cre}$- and AAV8-hDlx$^{ERT2\text{-}Cre}$-injected mice spend significantly less time exploring the displaced object compared with controls (Figures 6B and 6C). Consistent with this observation, the discrimination index was significantly reduced after *Adamtsl3* deletion in adult rodent brains.

We also investigated the possibility of a co-existing memory defect that is less reliant on the hippocampus using the novel object recognition test (NORT)[35,36] (Figure 6D). We found that *Adamtsl3*$^{flox/flox}$ mice injected with Cre virus could not discriminate between the familiar and the novel object (Figure S7B). Similarly, adult deletion of *Adamtsl3* in either pyramidal neurons or interneurons led the mice to spend equal time exploring the novel and the familiar object (Figures 6E and 6F). The discrimination index was also significantly reduced (Figures 6E and 6F). Combined, our behavioral data identify that Adamtsl3, via its direct influence on GABAergic synaptic plasticity, impairs hippocampus function underlying spatial and recognition memory.

DISCUSSION

Ce-Punctin secreted at the NMJ plays a central role in specifying the identity of excitatory versus inhibitory postsynaptic specializations in *C. elegans*.[11] In this study, we set out to

Figure 5. Adamtsl3 activates DCC and downstream Src to induce inhibitory synapse plasticity

(A) WB for DCC and pDCC after iLTP in AAV8-hSyn1-RFP (control)-infected cultures (n = 6).

(B) WB for DCC and pDCC after iLTP in AAV8-hSyn1-RFP-Cre (Cre)-infected cultures (n = 4–6).

(C) Left: control virus-infected cultures after iLTP stained for Adamtsl3 (green) and gephyrin (red). Right: quantification of puncta densities (n = 30–40 from 3 biological replicates).

(D) Left: Cre virus-infected cultures after iLTP stained for Adamtsl3 (green) and gephyrin (red). Right: quantification of puncta densities (n = 30–40 from 3 biological replicates).

(E) Left: control virus-infected cultures after cLTP stained for GluA1 (green) and PSD95 (red). Right: quantification of puncta densities (n = 30–40 from 3 biological replicates).

(F) Left: Cre virus-infected cultures after cLTP stained for GluA1 (green) and PSD95 (red). Right: quantification of puncta densities (n = 30–40 from 3 biological replicates).

(G) Left: control virus-infected cultures after iLTP in the presence of 20 μM PP1 (Src inhibitor) or vehicle control stained for gephyrin (red) and γ2 $GABA_AR$ (green). Right: quantification of cluster densities (n = 50–60 from 3 biological replicates). Scale bar, 5 μm. Data are shown as mean ± SD. *p < 0.05, **p < 0.01, ***p < 0.005, ****p < 0.001, as determined by Student's two-tailed t test.

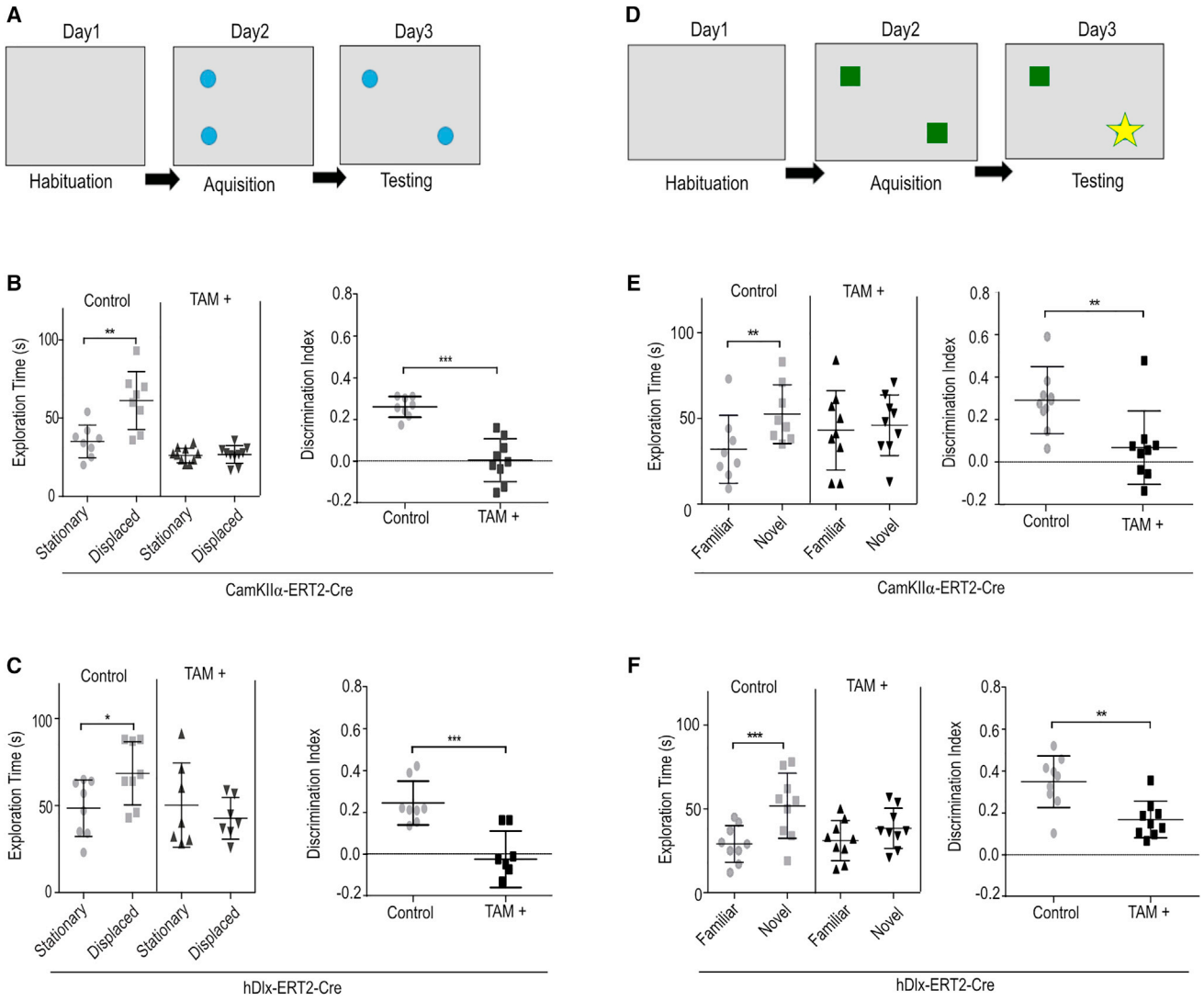

Figure 6. Neuron-specific deletion of Adamtsl3 in the adult brain impairs memory

(A) Illustration of object displacement test.

(B) Left: quantification of exploration time of AAV6-CaMKIIα-$^{ERT2\text{-}Cre}$-injected mice on testing day (control: n = 8; TAM$^+$: n = 10). Right: quantification of discrimination index (control: n = 8; TAM$^+$: n = 10).

(C) Left: quantification of exploration time of AAV8-hDlx-$^{ERT2\text{-}Cre}$-injected mice on testing day (control: n = 8; TAM$^+$: n = 7). Right: quantification of discrimination index (control: n = 8; TAM$^+$: n = 7).

(D) Illustration of novel object recognition test.

(E) Left: quantification of exploration time of AAV6-CaMKIIα-$^{ERT2\text{-}Cre}$-injected mice on testing day (control: n = 9; TAM$^+$: n = 9). Right: quantification of discrimination index (control: n = 9; TAM$^+$: n = 9).

(F) Left: quantification of exploration time of AAV8-hDlx-$^{ERT2\text{-}Cre}$-injected mice on testing day (control: n = 9; TAM$^+$: n = 9). Right: quantification of discrimination index (control: n = 9; TAM$^+$: n = 9).

Data are shown as mean ± SD. *p < 0.05, **p < 0.01, ***p < 0.005, as determined by Student's two-tailed t test.

characterize the Ce-Punctin ortholog, Adamtsl3, in the rodent brain. Similar to Ce-Punctin, we report that Adamtsl3 functions at both inhibitory and excitatory synaptic sites. In the early post-natal brain, Adamtsl3 facilitates DCC function for GABAergic and glutamatergic synapse formation. In the adult brain, Adamtsl3 signals via the DCC receptor to specifically influence GABAergic synapse maintenance, whereas Netrin-1 signals via DCC to influence glutamatergic synapse maintenance. Using neuronal-subtype-specific deletion of *Adamtsl3*, we uncover presynaptic and postsynaptic contributions of Adamtsl3 to DCC receptor signaling at GABAergic synapses, where presynaptic Adamtsl3 stabilizes/localizes DCC and postsynaptic Adamtsl3 activates DCC signaling for GABAergic synapse maintenance. Functionally, the Adamtsl3-DCC signaling module supports plasticity changes at GABAergic synapses through Src pathway activation. Along that line, behavioral

assays indicate that presynaptic and postsynaptic Adamtsl3 sustain hippocampal function in memory encoding. Together, our data identify Adamtsl3 as an extracellular synapse organizer at GABAergic synapses *in vivo*.

Beyond Netrin-1-DCC nexus

The cognate ligand for DCC has been Netrin-1. Commissural axons express DCC on their growth cones where Netrin-1 binding triggers intracellular signaling that directs the growth cone along a Netrin-1 gradient.[6,27] Growing evidence, however, suggests that the attractive function of Netrin-1 at DCC is region dependent[37] and further modulated by co-factors such as CD146[38] and glypicans.[39] In the rodent brain, axonal guidance is completed by P10,[40] and we anticipate our method of intracranial AAV8-hSyn1-RFP-Cre injection at P0 to cease Adamtsl3 expression only at P10 or later.[41] Therefore, *Adamtsl3* deletion is unlikely to influence axon guidance using our experimental paradigm. However, we also find *Adamtsl3* mRNA expression to be high in the hippocampal formation of BL6 mice at P5 (Figure S1F). Because Netrin-1 was shown to attract mossy fibers and regulate their directionality via DCC during the first postnatal week,[42] Adamtsl3 signaling at DCC may also influence axon targeting in the developing hippocampus. Importantly, the *C. elegans* ortholog of Adamtsl3, Ce-Punctin, was found to function redundantly with Netrin/UNC-6 in midline-oriented guidance.[43,44] Whether this functional redundancy is evolutionarily conserved in the rodent brain or whether Adamtsl3 signaling at DCC is independently involved in axon targeting remains to be determined.

Following axonal guidance, a surge in synapse formation occurs between P14 and P21, facilitating circuit maturation.[40,45] Netrin-1 and DCC signaling have been shown to facilitate the adhesion of putative synaptic contacts and focal accumulation of synaptic proteins through the reorganization of actin cytoskeleton effector proteins such as Nck1 (Dock), Pak1, Cdc42, Rac1, and RhoA at excitatory terminals.[25,46] However, Draxin,[37] Cerebellin 4,[47] DSCAM,[48] and heparan sulfates in the perisynaptic space[49] have also been implicated in facilitating DCC-dependent synaptogenesis. Our identification of Adamtsl3 as a DCC ligand influencing GABAergic and glutamatergic synapse formation adds further complexity to the *trans*-signaling network of DCC.

Interestingly, Adamtsl3-DCC interaction is evolutionarily conserved as *C. elegans* Ce-Punctin and UNC-40/DCC also physically interact to facilitate NMJ formation. Two isoforms have been characterized for *Ce-Punctin*, which are both ligands of UNC-40/DCC localized at cholinergic and/or GABAergic NMJs. In contrast, three *Adamtsl3* variants have been reported, of which we and others have detected only one in adult mice.[14,50] Using our homemade antibody, which permits immunohistochemical detection of all predicted isoforms, we identified preferential localization of Adamtsl3 at adult GABAergic synapses. However, we do not know whether Adamtsl3 isoforms are differentially expressed in early development and are perhaps also expressed at glutamatergic synapses interacting with DCC. Our observations from P0 *Adamtsl3* deletion and neuron-HEK293T co-culture assay support a function for Adamtsl3 in both excitatory and inhibitory synaptogenesis, suggesting that expression of Adamtsl3 isoforms is either spatiotemporally regulated or that Adamtsl3 cooperates with other ligands, such as Netrin-1, for glutamatergic synapse formation. The interplay between DCC, Adamtsl3, Netrin-1, and other signals for synapse formation and specification will thus require further clarification. At GABAergic synapses, investigating the spatiotemporal relationship between Adamtsl3-DCC and other known signaling molecules such as Slitrk3 (Slit and NTRK-like family member 3), PTPδ (tyrosine phosphatase receptor PTP delta),[51] and adenosine A_{2A} receptor[52] will also be essential to define the role of Adamtsl3.

Adamtsl3 ortholog Ce-Punctin was additionally shown to cluster NLG1 to facilitate the recruitment of $GABA_A$ receptors.[10] In our neuron-HEK293T co-culture assay, we examined VGAT-positive synapse formation and found the synaptogenic function of Adamtsl3 at DCC to be independent of NLG1 or NLG2 (Figures S3B and S3C). However, because we did not assess postsynaptic induction in our co-culture assay, we do not know whether Adamtsl3 is required for $GABA_A$ receptor clustering and whether it requires NLG2. Due to the lack of a good NLG2 commercial antibody, we could further not assess NLG2 expression changes using immunohistochemistry upon *Adamtsl3* gene deletion. Takahashi et al.[51] found that the postsynaptic adhesion molecule Slitrk3 efficiently induced VGAT-positive synapses independent of NLG2 in co-culture assay, but they noted that Slitrk3 and NLG2 cooperate *in vivo* to regulate the development of GABAergic synapses in CA1. A role for NLGs in Adamtsl3 function *in vivo* can thus not be excluded. In this regard, it is important to point out that *Adamtsl3* deletion early in post-natal development causes almost 50% loss of GABAergic synapses, such a strong effect has been documented only following the deletion of NLG2.[53] NLG2 deletion results in a region-specific loss of somatic $GABA_A$ receptors in CA1,[54] and *Adamtsl3* deletion results in functional impairment of GABAergic inhibition in CA1 pyramidal cells. It thus stands to reason that downstream signaling pathways of DCC and NLG2 cooperate or even overlap to promote $GABA_A$ receptor clustering. Notably, proteolysis of Ce-Punctin was recently shown to generate a shorter N-terminal fragment in *C. elegans*, which specifically binds NLG1 and contributes to the organization of GABAergic postsynaptic domains together with UNC-40/DCC.[10,55] Because we found the interaction between Adamtsl3 and DCC to be functionally conserved, proteolytic cleavage of Adamtsl3 may also be of relevance for NLG function and synapse specification in the mouse brain.

Adamtsl3-DCC signaling for GABAergic synapse maintenance

In the adult brain, DCC plays a key role in excitatory spine maintenance and GluN2B expression at synaptic sites. In addition, *DCC* deletion has been shown to cause deficits in LTP induction and spatial memory.[8] Here, we uncover a previously unanticipated role for DCC at GABAergic synapses. By deleting *DCC* in specific neuron subtypes, we found that DCC signals to maintain GABAergic presynaptic and postsynaptic compartments in a site-specific manner (Figures 4H and 4I). Our data are consistent with another report showing specific presynaptic and postsynaptic contributions of DCC to the electrophysiological

properties of excitatory synapses at CA1 pyramidal neurons.[28,29] However, it is intriguing that VGAT or gephyrin clusters are maintained after *DCC* is deleted at opposing presynaptic or postsynaptic sites (Figure 4I). *Trans*-synaptic interactions (e.g., Neurexin-NLG) are thought to dictate synapse specification and maintenance, but distinct mechanisms that induce either presynaptic or postsynaptic assemblies have also been identified.[5,56] How DCC signals to maintain specific GABAergic compartments remains to be investigated but likely involves downstream effectors of the synaptic cytoskeleton, including Nck1 (Dock), Pak1, or Rho GTPases (Cdc42, Rac1, and RhoA).[8,46,57]

By deleting *Adamtsl3* in specific neuron subtypes, we could delineate that Adamtsl3 from presynaptic and postsynaptic neurons is essential for maintaining CA1 GABAergic compartments. Whereas *Adamtsl3*$^{flox/flox}$ mice injected with AAV6-CaMKII$\alpha^{ERT2\text{-}Cre}$ show synapse changes restricted to the postsynaptic site, *Adamtsl3*$^{flox/flox}$ mice injected with AAV8-hDlx$^{ERT2\text{-}Cre}$ show compromised GABAergic neurotransmission at the level of presynaptic neurotransmitter release (IEI) and postsynaptic receptor availability (amplitude) (Figure 3G). Our data thus identify divergent roles for presynaptic and postsynaptic Adamtsl3 that act in a site-specific and *trans*-synaptic manner, respectively. Our data further indicate that these divergent roles are at least in part mediated by the differential contribution of presynaptic and postsynaptic Adamtsl3 to DCC receptor function. We propose a simple hypothesis in which presynaptic Adamtsl3 stabilizes DCC at postsynaptic GABAergic sites (Figure 4D) and in which postsynaptically released Adamtsl3 is essential for DCC activation in pyramidal cells (Figure 4F). One can envision a role for distinct post-translational modifications such as glycosylation to dictate how presynaptic and postsynaptic Adamtsl3 differentially bind and/or regulate DCC at the postsynaptic site. The mechanistic details, however, are currently missing.

The role of Adamtsl3 at presynaptically localized DCC will also require further investigation. Adult deletion of *Adamtsl3* from interneurons does not alter the puncta density of VGAT (Figure 3C), a marker for GABAergic terminals, whereas *DCC* deletion from interneurons decreases VGAT puncta density (Figure 4H). DCC must thus be stabilized (or activated) by a ligand different from Adamtsl3 for its role at GABAergic presynaptic sites. Yet, adult deletion of *Adamtsl3* from interneurons triggers a strong reduction in mIPSC IEIs (Figure 3G), which is indicative of presynaptic dysfunction. Netrin-1-DCC signaling has been shown to activate syntaxin-1, which together with SNAP25 and synaptobrevin-2 is required for vesicular mobilization and depolarization-mediated fusion at synapses.[58,59] *Adamtsl3* deletion from interneurons may thus alter presynaptic DCC function with consequences for neurotransmitter release. In support of this view, Glasgow et al.[29] found that *DCC* loss at excitatory terminals impaired evoked neurotransmission. At present, our findings indicate that presynaptic Adamtsl3 also influences presynaptic GABAergic activity possibly involving GABA release dynamics, but the specific mechanism and role of DCC in it require further investigation.

By silencing *Netrin-1* mRNA in the adult brain, we further provide evidence that Netrin-1 signaling at the DCC receptor in the mature brain specifically influences glutamatergic synapse integrity (Figure S6). What facilitates the segregation of Netrin-1-DCC and Adamtsl3-DCC signaling toward glutamatergic and GABAergic synapses, respectively, will require further investigation. Thus far, we do not know whether the divergent functions of Adamtsl3 and Netrin-1 are exclusively the result of synapse-specific expression patterns. Although we found preferential localization of Adamtsl3 at GABAergic synapses, we were not able to assess the synaptic localization of Netrin-1 using immunohistochemistry in the adult brain. Netrin-1 function at glutamatergic synapses is well described in the literature, but *Netrin-1* mRNA is also highly expressed in the CA1 *S. pyramidale* (data were derived from the Allen Mouse Brain Atlas In situ hybridization [ISH]), indicating that it may be present at CA1 GABAergic synapses. It thus remains to be determined whether DCC signaling at GABAergic synapses relies on the synergistic function of Adamtsl3 and Netrin-1 or solely on Adamtsl3. In particular, Adamtsl3 may be necessary to alter DCC-Netrin-1 signaling at GABAergic synapses: both CDK5 and GSK3β have been linked to reduced gephyrin scaffolding and microtubule interaction and are activated downstream of DCC-Netrin-1 signaling.[60–64] Adamtsl3 binding to DCC may thus displace or alter Netrin-1 signaling for GABAergic synapse maintenance. Altogether, our data indicate an essential role of Adamtsl3 in dynamically organizing the molecular architecture of GABAergic synapses in the hippocampus with functional consequences for synapse plasticity and memory (Figures 5 and 6).

Adamtsl3-DCC downstream effector facilitates GABAergic postsynaptic plasticity

Just like Netrin-1,[27,37] we have identified that Adamtsl3 can directly facilitate DCC Tyr1418 phosphorylation to activate downstream signaling. Using an *in vitro* paradigm of iLTP, we show that Adamtsl3 influences DCC and Src activation for adaptations in GABAergic inhibition (Figure S5). We anticipate that Adamtsl3-DCC-Src signaling acts directly on the $GABA_A$ receptor γ2 subunit at the previously characterized Tyr365/367 sites for hippocampal plasticity and memory function.[32,33] We do not expect Src to facilitate GABAergic synaptic plasticity through gephyrin because there are no Src consensus motifs on gephyrin for direct phosphorylation. However, other known DCC effectors such as CaMKIIα[65] or PLCγ1[45] have been implicated in inhibitory synapse function and could also modify the gephyrin scaffold and/or $GABA_A$ receptors downstream of Adamtsl3-DCC.[66] Lastly, the role of presynaptic Adamtsl3 in iLTP requires further investigation, because presynaptic DCC dysfunction and attenuated synaptic transmission following *Adamtsl3* deletion may contribute to impairing the expression of iLTP. *Adamtsl3* has been identified as a candidate gene for schizophrenia, which in turn has consistently been associated with reduced GABAergic neurotransmission.[67] The signaling cascade that we have outlined downstream of Adamtsl3 at GABAergic synapses is thus pivotal for understanding brain function in both health and disease.

Limitations of the study

A major limitation of the current study is that our homemade antibody against Adamtsl3 does not enable us to differentiate individual Adamtsl3 isoforms, which could exhibit specific functions.

We further used common synapse markers for IHC and were therefore unable to address the molecular heterogeneity of CA1 synapses; detailed morphological and functional analyses of other brain regions may also yield other biological findings. Lastly, we do not know the half-life of Adamtsl3 and the time to AAV8-hSyn1-RFP-Cre expression after P0 injection. Thus, we were unable to ascertain which developmental programs are influenced by Adamtsl3 in the early post-natal brain.

STAR★METHODS

Detailed methods are provided in the online version of this paper and include the following:

- KEY RESOURCES TABLE
- RESOURCE AVAILABILITY
  - Lead contact
  - Materials availability
  - Data and code availability
- EXPERIMENTAL MODEL AND SUBJECT DETAILS
- METHOD DETAILS
  - Primary neuron cultures
  - Preparation of HEK293T cells and neuron-HEK293T co-culture
  - Immunohistochemistry
  - Immunoprecipitation and WB
  - In situ proximity ligation assay (in situ PLA)
  - Synaptoneurosomes preparation
  - Slice preparation and electrophysiological recordings
  - iLTP and cLTP in primary neuron culture
  - Stereotactic surgery
  - Object displacement test and novel object recognition test
- QUANTIFICATION AND STATISTICAL ANALYSIS

SUPPLEMENTAL INFORMATION

Supplemental information can be found online at https://doi.org/10.1016/j.celrep.2023.112947.

ACKNOWLEDGMENTS

We thank Patrick Mehlen for generously providing *DCC*$^{flox/flox}$ mice; Prof. Alyson Fournier for sharing the pCMV-myc-DCC plasmid; Prof. Peter Scheiffele for sharing the HA-NLG2 and HA-NLG1 plasmids; and Jean-Charles Paterna and Melanie Rausch from the Viral Vector Core at the University of Zürich for viral vector cloning and virus production. We thank Prof. Jean-Marc Fritschy and the Bessereau lab members for their feedback on the manuscript. This study was supported by a UZH Forschungskredit Can-doc grant (to T.M.L.C.), as well as Swiss National Science Foundation grants (31003A_159867 and 310030_192522) and University of Zurich internal funding (to S.K.T.).

AUTHOR CONTRIBUTIONS

Conceptualization, T.M.L.C. and S.K.T.; methodology, T.M.L.C. and S.K.T.; investigation, T.M.L.C., Y.-C.T., A.C., A.D., M.A.B., T.K., and N.R.; writing – original draft, T.M.L.C. and S.K.T.; writing – review & editing, T.M.L.C., S.K.T., B.P.-L., and J.-L.B.; funding acquisition, T.M.L.C. and S.K.T.

DECLARATION OF INTERESTS

The authors declare no competing interests.

Received: February 22, 2023
Revised: June 23, 2023
Accepted: July 20, 2023
Published: August 10, 2023

REFERENCES

1. Fuccillo, M.V., Földy, C., Gökce, Ö., Rothwell, P.E., Sun, G.L., Malenka, R.C., and Südhof, T.C. (2015). Single-Cell mRNA Profiling Reveals Cell-Type-Specific Expression of Neurexin Isoforms. Neuron *87*, 326–340. https://doi.org/10.1016/j.neuron.2015.06.028.
2. Ichtchenko, K., Nguyen, T., and Südhof, T.C. (1996). Structures, Alternative Splicing, and Neurexin Binding of Multiple Neuroligins (*). J. Biol. Chem. *271*, 2676–2682. https://doi.org/10.1074/jbc.271.5.2676.
3. Siddiqui, T.J., Tari, P.K., Connor, S.A., Zhang, P., Dobie, F.A., She, K., Kawabe, H., Wang, Y.T., Brose, N., and Craig, A.M. (2013). An LRRTM4-HSPG Complex Mediates Excitatory Synapse Development on Dentate Gyrus Granule Cells. Neuron *79*, 680–695. https://doi.org/10.1016/j.neuron.2013.06.029.
4. Uemura, T., Lee, S.-J., Yasumura, M., Takeuchi, T., Yoshida, T., Ra, M., Taguchi, R., Sakimura, K., and Mishina, M. (2010). Trans-Synaptic Interaction of GluRδ2 and Neurexin through Cbln1 Mediates Synapse Formation in the Cerebellum. Cell *141*, 1068–1079. https://doi.org/10.1016/j.cell.2010.04.035.
5. Südhof, T.C. (2017). Synaptic Neurexin Complexes: A Molecular Code for the Logic of Neural Circuits. Cell *171*, 745–769. https://doi.org/10.1016/j.cell.2017.10.024.
6. Hérincs, Z., Corset, V., Cahuzac, N., Furne, C., Castellani, V., Hueber, A.-O., and Mehlen, P. (2005). DCC association with lipid rafts is required for netrin-1-mediated axon guidance. J. Cell Sci. *118*, 1687–1692. https://doi.org/10.1242/jcs.02296.
7. Liu, Y., Bhowmick, T., Liu, Y., Gao, X., Mertens, H.D.T., Svergun, D.I., Xiao, J., Zhang, Y., Wang, J.H., and Meijers, R. (2018). Structural Basis for Draxin-Modulated Axon Guidance and Fasciculation by Netrin-1 through DCC. Neuron *97*, 1261–1267.e4. https://doi.org/10.1016/j.neuron.2018.02.010.
8. Horn, K.E., Glasgow, S.D., Gobert, D., Bull, S.-J., Luk, T., Girgis, J., Tremblay, M.-E., McEachern, D., Bouchard, J.-F., Haber, M., et al. (2013). DCC Expression by Neurons Regulates Synaptic Plasticity in the Adult Brain. Cell Rep. *3*, 173–185. https://doi.org/10.1016/j.celrep.2012.12.005.
9. Stavoe, A.K.H., and Colón-Ramos, D.A. (2012). Netrin instructs synaptic vesicle clustering through Rac GTPase, MIG-10, and the actin cytoskeleton. J. Cell Biol. *197*, 75–88. https://doi.org/10.1083/jcb.201110127.
10. Tu, H., Pinan-Lucarré, B., Ji, T., Jospin, M., and Bessereau, J.-L. (2015). C. elegans Punctin Clusters GABA(A) Receptors via Neuroligin Binding and UNC-40/DCC Recruitment. Neuron *86*, 1407–1419. https://doi.org/10.1016/j.neuron.2015.05.013.
11. Pinan-Lucarré, B., Tu, H., Pierron, M., Cruceyra, P.I., Zhan, H., Stigloher, C., Richmond, J.E., and Bessereau, J.-L. (2014). C. elegans Punctin specifies cholinergic versus GABAergic identity of postsynaptic domains. Nature (London) *511*, 466–470. https://doi.org/10.1038/nature13313.
12. Zhou, X., Gueydan, M., Jospin, M., Ji, T., Valfort, A., Pinan-Lucarré, B., and Bessereau, J.-L. (2020). The netrin receptor UNC-40/DCC assembles a postsynaptic scaffold and sets the synaptic content of GABAA receptors. Nat. Commun. *11*, 2674. https://doi.org/10.1038/s41467-020-16473-5.
13. Kelwick, R., Desanlis, I., Wheeler, G.N., and Edwards, D.R. (2015). The ADAMTS (A Disintegrin and Metalloproteinase with Thrombospondin motifs) family. Genome Biol. *16*, 113. https://doi.org/10.1186/s13059-015-0676-3.

14. Hall, N.G., Klenotic, P., Anand-Apte, B., and Apte, S.S. (2003). ADAMTSL-3/punctin-2, a novel glycoprotein in extracellular matrix related to the ADAMTS family of metalloproteases. Matrix Biol. *22*, 501–510. https://doi.org/10.1016/s0945-053x(03)00075-1.

15. Dow, D.J., Huxley-Jones, J., Hall, J.M., Francks, C., Maycox, P.R., Kew, J.N.C., Gloger, I.S., Mehta, N.A.L., Kelly, F.M., Muglia, P., et al. (2011). ADAMTSL3 as a candidate gene for schizophrenia: Gene sequencing and ultra-high density association analysis by imputation. Schizophr. Res. *127*, 28–34. https://doi.org/10.1016/j.schres.2010.12.009.

16. Hirohata, S., Wang, L.W., Miyagi, M., Yan, L., Seldin, M.F., Keene, D.R., Crabb, J.W., and Apte, S.S. (2002). Punctin, a Novel ADAMTS-like Molecule, ADAMTSL-1, in Extracellular Matrix. J. Biol. Chem. *277*, 12182–12189. https://doi.org/10.1074/jbc.m109665200.

17. Campbell, B.F.N., and Tyagarajan, S.K. (2019). Cellular Mechanisms Contributing to the Functional Heterogeneity of GABAergic Synapses. Front. Mol. Neurosci. *12*, 187. https://doi.org/10.3389/fnmol.2019.00187.

18. Tang, X., Jaenisch, R., and Sur, M. (2021). The role of GABAergic signalling in neurodevelopmental disorders. Nat. Rev. Neurosci. *22*, 290–307. https://doi.org/10.1038/s41583-021-00443-x.

19. Kim, J.-Y., Grunke, S.D., Levites, Y., Golde, T.E., and Jankowsky, J.L. (2014). Intracerebroventricular viral injection of the neonatal mouse brain for persistent and widespread neuronal transduction. J. Vis. Exp. *51863*, 51863. https://doi.org/10.3791/51863.

20. Jahn, H.M., Kasakow, C.V., Helfer, A., Michely, J., Verkhratsky, A., Maurer, H.H., Scheller, A., and Kirchhoff, F. (2018). Refined protocols of tamoxifen injection for inducible DNA recombination in mouse astroglia. Sci. Rep. *8*, 5913. https://doi.org/10.1038/s41598-018-24085-9.

21. Tyagarajan, S.K., and Fritschy, J.-M. (2014). Gephyrin: a master regulator of neuronal function? Nat. Rev. Neurosci. *15*, 141–156. https://doi.org/10.1038/nrn3670.

22. Olsen, R.W., and Sieghart, W. (2009). GABA A receptors: subtypes provide diversity of function and pharmacology. Neuropharmacology *56*, 141–148. https://doi.org/10.1016/j.neuropharm.2008.07.045.

23. Biederer, T., and Scheiffele, P. (2007). Mixed-culture assays for analyzing neuronal synapse formation. Nat. Protoc. *2*, 670–676. https://doi.org/10.1038/nprot.2007.92.

24. Hill, G.W., Purcell, E.K., Liu, L., Velkey, J.M., Altschuler, R.A., and Duncan, R.K. (2012). Netrin-1-Mediated Axon Guidance in Mouse Embryonic Stem Cells Overexpressing Neurogenin-1. Stem Cell. Dev. *21*, 2827–2837. https://doi.org/10.1089/scd.2011.0437.

25. Goldman, J.S., Ashour, M.A., Magdesian, M.H., Tritsch, N.X., Harris, S.N., Christofi, N., Chemali, R., Stern, Y.E., Thompson-Steckel, G., Gris, P., et al. (2013). Netrin-1 Promotes Excitatory Synaptogenesis between Cortical Neurons by Initiating Synapse Assembly. J. Neurosci. *33*, 17278–17289. https://doi.org/10.1523/jneurosci.1085-13.2013.

26. Loh, K.H., Stawski, P.S., Draycott, A.S., Udeshi, N.D., Lehrman, E.K., Wilton, D.K., Svinkina, T., Deerinck, T.J., Ellisman, M.H., Stevens, B., et al. (2016). Proteomic Analysis of Unbounded Cellular Compartments: Synaptic Clefts. Cell *166*, 1295–1307.e21. https://doi.org/10.1016/j.cell.2016.07.041.

27. Boyer, N.P., and Gupton, S.L. (2018). Revisiting Netrin-1: One Who Guides (Axons). Front. Cell. Neurosci. *12*, 221. https://doi.org/10.3389/fncel.2018.00221.

28. Glasgow, S.D., Labrecque, S., Beamish, I.V., Aufmkolk, S., Gibon, J., Han, D., Harris, S.N., Dufresne, P., Wiseman, P.W., McKinney, R.A., et al. (2018). Activity-Dependent Netrin-1 Secretion Drives Synaptic Insertion of GluA1-Containing AMPA Receptors in the Hippocampus. Cell Rep. *25*, 168–182.e6. https://doi.org/10.1016/j.celrep.2018.09.028.

29. Glasgow, S.D., Wong, E.W., Thompson-Steckel, G., Marcal, N., Séguéla, P., Ruthazer, E.S., and Kennedy, T.E. (2020). Pre- and post-synaptic roles for DCC in memory consolidation in the adult mouse hippocampus. Mol. Brain *13*, 56. https://doi.org/10.1186/s13041-020-00597-2.

30. Petrini, E.M., Ravasenga, T., Hausrat, T.J., Iurilli, G., Olcese, U., Racine, V., Sibarita, J.-B., Jacob, T.C., Moss, S.J., Benfenati, F., et al. (2014). Synaptic recruitment of gephyrin regulates surface GABAA receptor dynamics for the expression of inhibitory LTP. Nat. Commun. *5*, 3921. https://doi.org/10.1038/ncomms4921.

31. McLeod, F., Bossio, A., Marzo, A., Ciani, L., Sibilla, S., Hannan, S., Wilson, G.A., Palomer, E., Smart, T.G., Gibb, A., and Salinas, P.C. (2018). Wnt Signaling Mediates LTP-Dependent Spine Plasticity and AMPAR Localization through Frizzled-7 Receptors. Cell Rep. *23*, 1060–1071. https://doi.org/10.1016/j.celrep.2018.03.119.

32. Brandon, N.J., Delmas, P., Hill, J., Smart, T.G., and Moss, S.J. (2001). Constitutive tyrosine phosphorylation of the GABAA receptor γ2 subunit in rat brain. Neuropharmacology *41*, 745–752. https://doi.org/10.1016/s0028-3908(01)00121-6.

33. Moss, S.J., Smart, T.G., Blackstone, C.D., and Huganir, R.L. (1992). Functional modulation of GABAA receptors by cAMP-dependent protein phosphorylation. Science (New York, N.Y.) *257*, 661–665.

34. Wong, E.W., Glasgow, S.D., Trigiani, L.J., Chitsaz, D., Rymar, V., Sadikot, A., Ruthazer, E.S., Hamel, E., and Kennedy, T.E. (2019). Spatial memory formation requires netrin-1 expression by neurons in the adult mammalian brain. Learn. Mem. *26*, 77–83. https://doi.org/10.1101/lm.049072.118.

35. Denninger, J.K., Smith, B.M., and Kirby, E.D. (2018). Novel Object Recognition and Object Location Behavioral Testing in Mice on a Budget. J. Vis. Exp. https://doi.org/10.103791/58593.

36. Antunes, M., and Biala, G. (2012). The novel object recognition memory: neurobiology, test procedure, and its modifications. Cognit. Process. *13*, 93–110. https://doi.org/10.1007/s10339-011-0430-z.

37. Meijers, R., Smock, R.G., Zhang, Y., and Wang, J.-H. (2020). Netrin Synergizes Signaling and Adhesion through DCC. Trends Biochem. Sci. *45*, 6–12. https://doi.org/10.1016/j.tibs.2019.10.005.

38. Tu, T., Zhang, C., Yan, H., Luo, Y., Kong, R., Wen, P., Ye, Z., Chen, J., Feng, J., Liu, F., et al. (2015). CD146 acts as a novel receptor for netrin-1 in promoting angiogenesis and vascular development. Cell Res. *25*, 275–287. https://doi.org/10.1038/cr.2015.15.

39. Blanchette, C.R., Perrat, P.N., Thackeray, A., and Bénard, C.Y. (2015). Glypican Is a Modulator of Netrin-Mediated Axon Guidance. PLoS Biol. *13*, e1002183. https://doi.org/10.1371/journal.pbio.1002183.

40. Pelkey, K.A., Chittajallu, R., Craig, M.T., Tricoire, L., Wester, J.C., and McBain, C.J. (2017). Hippocampal GABAergic Inhibitory Interneurons. Physiol. Rev. *97*, 1619–1747. https://doi.org/10.1152/physrev.00007.2017.

41. Kim, Y.-E., Kim, S., and Kim, I.H. (2022). Neural circuit-specific gene manipulation in mouse brain in vivo using the split-intein-mediated split-Cre system. STAR Protoc. *3*, 101807. https://doi.org/10.1016/j.xpro.2022.101807.

42. Muramatsu, R., Nakahara, S., Ichikawa, J., Watanabe, K., Matsuki, N., and Koyama, R. (2010). The ratio of 'deleted in colorectal cancer' to 'uncoordinated-5A' netrin-1 receptors on the growth cone regulates mossy fibre directionality. Brain *133*, 60–75. https://doi.org/10.1093/brain/awp266.

43. Seetharaman, A., Selman, G., Puckrin, R., Barbier, L., Wong, E., D'Souza, S.A., and Roy, P.J. (2011). MADD-4 Is a Secreted Cue Required for Midline-Oriented Guidance in Caenorhabditis elegans. Dev. Cell *21*, 669–680. https://doi.org/10.1016/j.devcel.2011.07.020.

44. Zhou, X., and Bessereau, J.-L. (2019). Molecular Architecture of Genetically-Tractable GABA Synapses in C. elegans. Front. Mol. Neurosci. *12*, 304. https://doi.org/10.3389/fnmol.2019.00304.

45. Kim, H.Y., Yang, Y.R., Hwang, H., Lee, H.-E., Jang, H.-J., Kim, J., Yang, E., Kim, H., Rhim, H., Suh, P.-G., and Kim, J.I. (2019). Deletion of PLCγ1 in GABAergic neurons increases seizure susceptibility in aged mice. Sci. Rep. *9*, 17761. https://doi.org/10.1038/s41598-019-54477-4.

46. Tada, T., and Sheng, M. (2006). Molecular mechanisms of dendritic spine morphogenesis. Curr. Opin. Neurobiol. *16*, 95–101. https://doi.org/10.1016/j.conb.2005.12.001.

47. Haddick, P.C.G., Tom, I., Luis, E., Quiñones, G., Wranik, B.J., Ramani, S.R., Stephan, J.-P., Tessier-Lavigne, M., and Gonzalez, L.C. (2014). Defining the Ligand Specificity of the Deleted in Colorectal Cancer (DCC) Receptor. PLoS One *9*, e84823. https://doi.org/10.1371/journal.pone.0084823.

48. Santos, R.A., Fuertes, A.J.C., Short, G., Donohue, K.C., Shao, H., Quintanilla, J., Malakzadeh, P., and Cohen-Cory, S. (2018). DSCAM differentially modulates pre- and postsynaptic structural and functional central connectivity during visual system wiring. Neural Dev. *13*, 22. https://doi.org/10.1186/s13064-018-0118-5.

49. Smock, R.G., and Meijers, R. (2018). Roles of glycosaminoglycans as regulators of ligand/receptor complexes. Open Biol. *8*, 180026. https://doi.org/10.1098/rsob.180026.

50. Rypdal, K.B., Olav Melleby, A., Robinson, E.L., Li, J., Palmero, S., Seifert, D.E., Martin, D., Clark, C., López, B., Andreassen, K., et al. (2022). ADAMTSL3 knock-out mice develop cardiac dysfunction and dilatation with increased TGFβ signalling after pressure overload. Commun. Biol. *5*, 1392. https://doi.org/10.1038/s42003-022-04361-1.

51. Takahashi, H., Katayama, K.I., Sohya, K., Miyamoto, H., Prasad, T., Matsumoto, Y., Ota, M., Yasuda, H., Tsumoto, T., Aruga, J., and Craig, A.M. (2012). Selective control of inhibitory synapse development by Slitrk3-PTPδ trans-synaptic interactionS1-S2. Nat. Neurosci. *15*, 389–398. https://doi.org/10.1038/nn.3040

52. Gomez-Castro, F., Zappettini, S., Pressey, J.C., Silva, C.G., Russeau, M., Gervasi, N., Figueiredo, M., Montmasson, C., Renner, M., Canas, P.M., et al. (2021). Convergence of adenosine and GABA signalling for synapse stabilization during development. Science *374*, eabk2055. https://doi.org/10.1126/science.abk2055.

53. Gibson, J.R., Huber, K.M., and Südhof, T.C. (2009). Neuroligin-2 deletion selectively decreases inhibitory synaptic transmission originating from fast-spiking but not from somatostatin-positive interneurons. J. Neurosci. *29*, 13883–13897. https://doi.org/10.1523/jneurosci.2457-09.2009.

54. Poulopoulos, A., Aramuni, G., Meyer, G., Soykan, T., Hoon, M., Papadopoulos, T., Zhang, M., Paarmann, I., Fuchs, C., Harvey, K., et al. (2009). Neuroligin 2 drives postsynaptic assembly at perisomatic inhibitory synapses through gephyrin and collybistin. Neuron *63*, 628–642. https://doi.org/10.1016/j.neuron.2009.08.023.

55. Platsaki, S., Zhou, X., Pinan-Lucarré, B., Delauzun, V., Tu, H., Mansuelle, P., Fourquet, P., Bourne, Y., Bessereau, J.-L., and Marchot, P. (2020). The Ig-like domain of Punctin/MADD-4 is the primary determinant for interaction with the ectodomain of neuroligin NLG-1. J. Biol. Chem. *295*, 16267–16279. https://doi.org/10.1074/jbc.ra120.014591.

56. Scheiffele, P., Fan, J., Choih, J., Fetter, R., and Serafini, T. (2000). Neuroligin expressed in nonneuronal cells triggers presynaptic development in contacting axons. Cell *101*, 657–669.

57. Lai Wing Sun, K., Correia, J.P., and Kennedy, T.E. (2011). Netrins: versatile extracellular cues with diverse functions. Development *138*, 2153–2169. https://doi.org/10.1242/dev.044529.

58. Ros, O., Barrecheguren, P.J., Cotrufo, T., Schaettin, M., Roselló-Busquets, C., Vílchez-Acosta, A., Hernaiz-Llorens, M., Martínez-Marmol, R., Ulloa, F., Stoeckli, E.T., et al. (2018). A conserved role for Syntaxin-1 in pre- and post-commissural midline axonal guidance in fly, chick, and mouse. PLoS Genet. *14*, e1007432. https://doi.org/10.1371/journal.pgen.1007432.

59. Südhof, T.C., and Rothman, J.E. (2009). Membrane Fusion: Grappling with SNARE and SM Proteins. Science *323*, 474–477. https://doi.org/10.1126/science.1161748.

60. Del Río, J.A., González-Billault, C., Ureña, J.M., Jiménez, E.M., Barallobre, M.J., Pascual, M., Pujadas, L., Simó, S., La Torre, A., Wandosell, F., et al. (2004). MAP1B Is Required for Netrin 1 Signaling in Neuronal Migration and Axonal Guidance. Curr. Biol. *14*, 840–850. https://doi.org/10.1016/j.cub.2004.04.046.

61. Tyagarajan, S.K., Ghosh, H., Yévenes, G.E., Imanishi, S.Y., Zeilhofer, H.U., Gerrits, B., and Fritschy, J.-M. (2013). Extracellular signal-regulated kinase and glycogen synthase kinase 3β regulate gephyrin postsynaptic aggregation and GABAergic synaptic function in a calpain-dependent mechanism. J. Biol. Chem. *288*, 9634–9647. https://doi.org/10.1074/jbc.m112.442616.

62. Ghosh, H., Auguadri, L., Battaglia, S., Simone Thirouin, Z., Zemoura, K., Messner, S., Acuña, M.A., Wildner, H., Yévenes, G.E., Dieter, A., et al. (2016). Several posttranslational modifications act in concert to regulate gephyrin scaffolding and GABAergic transmission. Nat. Commun. *7*, 13365. https://doi.org/10.1038/ncomms13365.

63. Kuhse, J., Kalbouneh, H., Schlicksupp, A., Mükusch, S., Nawrotzki, R., and Kirsch, J. (2012). Phosphorylation of gephyrin in hippocampal neurons by cyclin-dependent kinase CDK5 at Ser-270 is dependent on collybistin. J. Biol. Chem. *287*, 30952–30966. https://doi.org/10.1074/jbc.m112.349597.

64. Zacchi, P., Antonelli, R., and Cherubini, E. (2014). Gephyrin phosphorylation in the functional organization and plasticity of GABAergic synapses. Front. Cell. Neurosci. *8*, 103. https://doi.org/10.3389/fncel.2014.00103.

65. de Luca, E., Ravasenga, T., Petrini, E.M., Polenghi, A., Nieus, T., Guazzi, S., and Barberis, A. (2017). Inter-Synaptic Lateral Diffusion of GABAA Receptors Shapes Inhibitory Synaptic Currents. Neuron *95*, 63–69.e5. https://doi.org/10.1016/j.neuron.2017.06.022.

66. Flores, C.E., Nikonenko, I., Mendez, P., Fritschy, J.-M., Tyagarajan, S.K., and Muller, D. (2015). Activity-dependent inhibitory synapse remodelling through gephyrin phosphorylation. Proc. Natl. Acad. Sci. USA *112*, E65–E72. https://doi.org/10.1073/pnas.1411170112.

67. Tanaka, S. (2008). Dysfunctional GABAergic inhibition in the prefrontal cortex leads to "psychotic" hyperactivation. BMC Neurosci. *9*, 41. https://doi.org/10.1186/1471-2202-9-41.

68. Krimpenfort, P., Song, J.-Y., Proost, N., Zevenhoven, J., Jonkers, J., and Berns, A. (2012). Deleted in colorectal carcinoma suppresses metastasis in p53-deficient mammary tumours. Nature *482*, 538–541. https://doi.org/10.1038/nature10790.

69. Kim, J.-Y., Ash, R.T., Ceballos-Diaz, C., Levites, Y., Golde, T.E., Smirnakis, S.M., and Jankowsky, J.L. (2013). Viral transduction of the neonatal brain delivers controllable genetic mosaicism for visualising and manipulating neuronal circuits in vivo. Eur. J. Neurosci. *37*, 1203–1220. https://doi.org/10.1111/ejn.12126.

70. Früh, S., Tyagarajan, S.K., Campbell, B., Bosshard, G., and Fritschy, J.-M. (2018). The catalytic function of the gephyrin-binding protein IQSEC3 regulates neurotransmitter-specific matching of pre- and post-synaptic structures in primary hippocampal cultures. J. Neurochem. *147*, 477–494. https://doi.org/10.1111/jnc.14572.

71. Noya, S.B., Colameo, D., Brüning, F., Spinnler, A., Mircsof, D., Opitz, L., Mann, M., Tyagarajan, S.K., Robles, M.S., and Brown, S.A. (2019). The forebrain synaptic transcriptome is organized by clocks but its proteome is driven by sleep. Science *366*, eaav2642. https://doi.org/10.1126/science.aav2642.

72. Fortin, D.A., Davare, M.A., Srivastava, T., Brady, J.D., Nygaard, S., Derkach, V.A., and Soderling, T.R. (2010). Long-term potentiation-dependent spine enlargement requires synaptic Ca2+-permeable AMPA receptors recruited by CaM-kinase I. J. Neurosci. *30*, 11565–11575. https://doi.org/10.1523/jneurosci.1746-10.2010.

73. Stamatakou, E., Marzo, A., Gibb, A., and Salinas, P.C. (2013). Activity-Dependent Spine Morphogenesis: A Role for the Actin-Capping Protein Eps8. J. Neurosci. *33*, 2661–2670. https://doi.org/10.1523/jneurosci.0998-12.2013.

STAR★METHODS

KEY RESOURCES TABLE

REAGENT or RESOURCE	SOURCE	IDENTIFIER
Antibodies		
Mouse monoclonal anti-Actin	Millipore	Cat no. MAB1501; RRID:AB_2223041
Rabbit polyclonal anti-Adamtsl3	Home-made	N/A
Rabbit polyclonal anti-Cre	Biolegend	Cat no. PRB-106P
Mouse monoclonal anti-DCC	Creative Diagnostics	Cat no. CABTL-956
Mouse monoclonal anti-DCC	BD bioscience	Cat no. G97-449; RRID:AB_395314
Rabbit polyclonal anti-phospho-DCC (Tyr1418)	Merck	Cat no. ABC1466
Rabbit polyclonal anti-ERK1/2	Sigma-Aldrich	Cat no. M5670; RRID:AB_477216
Rabbit polyclonal anti-ERK1/2 (Thr202/Tyr204)	Sigma-Aldrich	Cat no. M9692; RRID:AB_260729
Guinea pig polyclonal anti-GABAAR γ2	Home-made	N/A
Mouse monoclonal anti-Gephyrin	Synaptic Systems	Cat no. 147 111; RRID:AB_887719
Rabbit polyclonal anti-Gephyrin	Synaptic Systems	Cat no. 147 008; RRID:AB_2619834
Rabbit polyclonal anti-GFP	Synaptic Systems	Cat no. 132 002; RRID:AB_887725
Rat monoclonal anti-HA (3F10)	Roche/Sigma	Cat no. 11 867 423 001
Goat polyclonal anti-Homer-1a	Santa Cruz	Cat no. SC-8922; RRID:AB_675651
Mouse monoclonal anti-myc (9E10)	Roche/Sigma	Cat no. 11 667 149 001
Guinea pig polyclonal anti-Parvalbumin	Immunostar	Cat no. 24428; RRID:AB_572259
Mouse monoclonal anti-PSD95	NeuroMap	Cat no. 73-028; RRID:AB_10698024
Mouse monoclonal anti-Somatostatin	ABOnline	Cat no. ABIN5662120
Rabbit polyclonal anti-Src	Cell Signaling Technology	Cat no. 2108; RRID:AB_331137
Rabbit polyclonal anti-Phospho-Src (Tyr416)	Cell Signaling Technology	Cat no. 2101; RRID:AB_331697
Guinea pig monoclonal anti-VGAT	Synaptic Systems	Cat no. 131 004; RRID:AB_887873
Guinea pig polyclonal anti-VGLUT1	Synaptic Systems	Cat no. 135 304; RRID:AB_887878
Bacterial and virus strains		
AAV8- hSyn1-RFP-Cre	Viral Vector Facility, UZH/ETH	Cat no. v230
AAV8- hSyn1-RFP	Viral Vector Facility, UZH/ETH	Cat no. v133
AAV8- hDlx-ERT2-Cre	Viral Vector Facility, UZH/ETH	Cat no. v301
AAV6- CAMKIIa-ERT2-Cre	Vector biolabs	Cat no. 2014-1208
AAV8-hSyn1-ShRNA-NTN1	Viral Vector Facility, UZH/ETH	Cat no. vTC2
AAV8-hSyn1-ShRNA-scramble	Viral Vector Facility, UZH/ETH	Cat no. V308
Chemicals, peptides, and recombinant proteins		
Neurobasal Plus media	Thermo Fisher Scientific	Cat no. 836
Tamoxifen	Sigma	Cat no. T5648
EvaGreen mastermix	Seraglob	Cat no. 1905-522
Complete Mini Protease Inhibitor	Roche	Cat no. 1183617001
Phosphatase inhibitor cocktail 2, 3	Sigma	Cat no. P0044, p5926
Pierce Protein A/G Ultralink Resin	Thermo Fischer	Cat no. 53132
Percoll	GE Healthcare,	Cat no. 17-0891-01
L-Glutamine Polyethylenimine Hydrochloride	Thermo Fischer	Cat no. 25030-032
Polyethylenimine	Polysciences	Cat no. 25439
Western Blocking Reagent	Roche	Cat no. 11921673001
SuperSignal™ West Pico PLUS Chemiluminescent Substrate	Thermo Fischer	Cat no. 34577
Tetrodotoxin	Sigma	Cat no. 4368-28-9

(*Continued on next page*)

Continued

REAGENT or RESOURCE	SOURCE	IDENTIFIER
CNXQ	Tocris	Cat no. 0190
(N-Methyl-D-aspartic acid) NMDA	Sigma	Cat no. 6384-92-5
D-APV	Tocris	Cat no. 0106
Strychnine	Sigma	Cat no. 57-24-9
Bicuculline	Tocris	Cat no. 0130
Critical commercial assays		
PrimeScript™ Double Strand cDNA Synthesis Kit	Takara	Cat no. 6111A
GenElute™Total RNA Purification Kit	Sigma	Cat no. RNB100
Experimental models: Cell lines		
Human: HEK293T	ATCC	Cat no. CRL-3216
Experimental models: Organisms/strains		
Mouse:C57BL/6JCrl	Charles River Laboratories (Germany)	RRID IMSR_JAX:000664,
Mouse: Adamtsl3$^{flox/flox}$	Qiagen	N/A
Mouse: DCC$^{flox/flox}$	Krimpenfort et al.,[68]	N/A
Recombinant DNA		
Plasmid: C-terminal eGFP-tagged Adamtsl3	Berangere Pinan-Lucarre	N/A
Plasmid: N-terminal myc-tagged DCC	Natalie LaMarche	N/A
Plasmid: C-terminal eGFP-tagged N-cadherin	Addgene	Cat no.18870
Plasmid: N-terminal HA-tagged Neuroligin2A	Peter Scheiffele	N/A
Plasmid: N-terminal HA-tagged Neuroligin1	Peter Scheiffele	N/A
Primer: GAPDH Fwd	Microsynth	5′-CATCACTGCCACCCAGAAGACTG-3′
Primer: GAPDH Rev	Microsynth	5′-ATGCCAGTGAGCTTCCCGTTCAG-3′
Primer: Adamtsl3 Fwd	Microsynth	5′-CTTGTTCCCACAACAGCTCC-3′
Primer: Adamtsl3 Rev	Microsynth	5′-CGTGCAGTTTCTATCACAGGA-3′
Primer: Netrin-1 Fwd	Microsynth	5′-GGGGGTGTCTGTCTCAACTG-3′
Primer: Netrin-1 Rev	Microsynth	5′-GGCGCTACAGGAATCTTAATGC-3′
Software and algorithms		
Synaptic cluster analysis Python-script ImageJ	Cramer et al., 2022	https://doi.org/10.5281/zenodo.8167635

RESOURCE AVAILABILITY

Lead contact

Further information and requests for resources and reagents should be directed to and will be fulfilled by the lead contact, Shiva K. Tyagarajan (shiva.tyagarajan@gmail.com).

Materials availability

All reagents newly generated in this study are available from the lead contact without restriction.

Data and code availability

- All data reported in this paper will be shared by the lead contact upon request.
- The custom Python script using the ImageJ image-processing framework is openly available on a GitHub repository: https://github.com/PDKlab/Exocytose-EventsDetection All original code has been deposited at Zenodo and is publicly available as of the date of publication. DOIs are listed in the key resources table.
- Any additional information required to reanalyze the data reported in this work paper is available from the lead contact upon request.

EXPERIMENTAL MODEL AND SUBJECT DETAILS

The study was conducted per the guidelines set by the European Community Council Directives of November 24, 1986 (86/609/EEC) and approved by the cantonal veterinary office of Zurich and the Animal Resource Committee of the University of Lyon. All

procedures fulfilled the ARRIVE guidelines on experimental design, animal allocation to different experimental groups, blinding of samples to data analysis and reporting animal experiments. *Adamtsl3*$^{flox/flox}$ mice with conditional alleles carrying *loxP* sites in exon 2 were generated using CRISPR/cas9 (Cyagen, USA) in BL6 background. *DCC*$^{flox/flox}$ mice with conditional alleles carrying *loxP* sites in exon 23 were generated by Anton Berns[68] and generously provided to us by Prof. Patrick Mehlen, University of Lyon. To generate *Adamtsl3* knock-out, we employed lateral ventricle P0 injection.[69] P0 *Adamtsl3*$^{flox/flox}$ pups were intracranially injected with AAV8 expressing red-fluorescent protein (RFP) or RFP-Cre under the control of the human synapsin promoter (AAV8-hSyn1-RFP or AAV8-hSyn1-RFP-Cre). The injection sites were identified at 2/5 of the distance from the lambda suture to each eye located approximately 0.8–1 mm lateral from the sagittal suture, halfway between lambda and bregma. P0 AAV8-hSyn1-RFP or AAV8-hSyn1-RFP-Cre injections were assigned at random to littermates from homozygous breeding. Compared to *Adamtsl3*-$^{flox/flox}$/AAV8-hSyn1-RFP mice, *Adamtsl3*$^{flox/flox}$/AAV8-hSyn1-RFP-Cre mice showed a slight increase in average body weight with no other gross abnormalities. Adult *Adamtsl3* and *DCC* knock-out mice were generated by P0 *Adamtsl3*$^{flox/flox}$ and P0 *DCC*$^{flox/flox}$ lateral ventricle injection of AAV expressing tamoxifen-inducible Cre. ERT2-Cre expression under the control of the human synapsin promoter allowed for the inducible ablation of *Adamtsl3* in all neuronal cells (AAV8-hSyn1$^{ERT2-Cre}$). ERT2-Cre expression under the control of the CaMKIIα promoter and hDlx promoter allowed for the selective, inducible ablation of Adamtsl3 in excitatory or inhibitory neuronal cells respectively (AAV6-CaMKII$\alpha^{ERT2-Cre}$ and AAV8-hDlx$^{ERT2-Cre}$).

All AAV8 recombinant viruses were generated by the Viral Vector Core at the University of Zürich. The AAV6-CaMKII$\alpha^{ERT2Cre}$ virus was purchased from Vector Biolabs (#2014-1208). AAV injections were assigned at random to littermates from homozygous breeding. Mice were injected (i.p.) for five consecutive days with tamoxifen dissolved in corn oil (Sigma T5648; 1mg/day) to induce Cre recombinase activity from ERT2-Cre at 8 weeks and sacrificed at 12–14 weeks of age. Control animals were injected with vehicle alone. Animals receiving tamoxifen (TAM+) were assigned at random and both genders were used for all conditions. Adult *Adamtsl3* and *DCC* knock-out mice showed no gross abnormalities. All mouse lines were fed water and food under ab libitum conditions and housed in a 12 h light/dark cycle.

METHOD DETAILS

Primary neuron cultures

Dissociated hippocampal cells were prepared from *Adamtsl3*$^{flox/flox}$ pups.[70] At P0-1 the brains of decapitated *Adamtsl3*$^{flox/flox}$ pups were removed, the meninges were detached and the hippocampi were dissected using forceps on ice. Hippocampal neurons were then dissociated and plated on poly-L-lysine-coated, 18-mm glass coverslips (90,000 cells per coverslip). Cells were maintained in Neurobasal Plus media supplemented with B27 Plus and 2 mM L-Glutamine (all 836 from Thermo Fisher Scientific) in a 5% CO_2 incubator at 37°C. At 4 days *in vitro* (DIV), neuronal cultures were infected with AAV8-hSyn1-RFP-Cre (AAV8-hSyn1-RFP control) to delete *Adamtsl3* gene or AAV8-Syn1-shRNA-NTN1 (AAV8-hSyn1-shRNA-scramble control) to knock-down *Netrin-1* mRNA. Sigma's GenElute Total RNA Purification Kit (RNB100) was used to isolate RNA from infected neurons at 14DIV and at P5, P9, P15, and P30 from cortical, cerebellar and hippocampal BL6 lysates. Takara's cDNA Synthesis Kit was used to construct cDNA. RT-PCR using EvaGreen master mix (1905-522, Seraglob) was performed to assess *Adamtsl3* and *Netrin-1* mRNA expression.

Preparation of HEK293T cells and neuron-HEK293T co-culture

HEK293T cells were cultured in T75 flasks in DMEM, supplemented with 10%FBS and maintained in a 5% CO_2 incubator at 37°C. Cells were passaged as required. Before transfection, HEK293T cells were dissociated using trypsin and plated onto 35 mm culture dishes at a 5000 cells/dish density. Following overnight incubation, cultures at 40% confluency were transfected with 1μg of plasmid using the transfection agent polyethyleneimine (Polysciences Inc.) as suggested by the manufacturer. Plasmids: N-Cadherin-EGFP (Addgene #18870), HA- Neuroligin2 and HA-Neuroligin1 (gift from Prof. Peter Scheiffele, Biozentrum), pCMV-myc-DCC (gift from Prof. Nathalie Lamarche-Vane and Prof. Alyson Fournier, McGill University), pBP84-GFP-Adamtsl3 was subcloned from mouse cDNA and sequence confirmed. 48 h after transfection, HEK293T cells were detached and resuspended in Neurobasal Plus media with B27 Plus and 2 mM L-Glutamine supplemented with 2-AraC. Dissociated HEK293T cells were seeded atop hippocampal neurons (30,000 cells per coverslip) at 7DIV. Co-cultures were then returned to the incubator for 48 h to facilitate synapse recruitment. Coverslips were fixed in 4% paraformaldehyde for 10 min at room temperature, permeabilized with 0.1% Triton X-100 in PBS containing 10% normal goat serum, and stained using desired primary antibodies (key resources table) for 90 min at room temperature. Goat anti-Alexa 488 (Molecular Probes), goat anti-Cy3, and goat anti-Cy5 (Jackson Immunoresearch) were used to label the proteins for immunofluorescence. All secondary antibodies used were diluted at 1:500. Coverslips were mounted on glass slides using fluorescence mounting medium (DAKO). z stack images (4 optical sections, 0.5μm step size) were acquired using confocal laser scanning microscopy (LSM 700, Carl Zeiss). Images were taken using a 40× objective with a numerical aperture of 1.4, and pixel size of 112 nm^2. All imaging parameters were kept constant across conditions. A custom Python script using the ImageJ image-processing framework was used for puncta analysis. The script can be used as a plugin and is openly available on a GitHub repository (https://github.com/dcolam/Cluster-Analysis-Plugin). Representative example images were processed using ImageJ. Statistical tests were performed using Prism software (GraphPad).

Immunohistochemistry

All mice were anesthetized (Nembutal; 50 mg/kg i.p.) and perfused at 12–14 weeks with ice-cold artificial cerebrospinal fluid (ACSF; 125 mM NaCl, 2.5 mM KCl, 1.25 mM NaH_2PO_4, 26 mM $NaHCO_3$, 25 mM D-glucose, 2.5 mM $CaCl_2$, and 2 mM $MgCl_2$), which had been oxygenated (95% O_2, 5% CO_2) for 15 min. After removal, the brains were immediately fixed in 4% PFA for 90 min at 4°C. After rinsing in PBS, brains were incubated in 30% sucrose (in PBS) at 4°C overnight for cryo-protection. The frozen brains were cut into 40 μm thick coronal sections using a sliding microtome for immunohistochemistry and stored in the anti-freeze buffer. Sections covering the hippocampal formation were selected and after 3 × 10 min washes in Tris-Triton Solution (50mM Tris, 150mM NaCl, 0.05% Triton X-100, pH 7.4), sections were incubated in desired primary antibody (key resources table) solution (50mM Tris, 150mM NaCl, 0.4% Triton X-100, 2% normal goat serum, pH 7.4) at 4°C overnight. Sections were then washed 3 × 10 min in Tris-Triton Solution and incubated in secondary antibody solution (50mM Tris, 150mM NaCl, 0.05% Triton X-100, 2% normal goat serum, pH 7.4) for 30 min at room temperature with secondary antibodies. Goat anti-Alexa 488 (Molecular Probes), goat anti-Cy3, and goat anti-Cy5 (Jackson Immunoresearch) were used to label the proteins for immunofluorescence. All secondary antibodies used were diluted at 1:500. Sections were washed 3 × 10 min in Tris-Triton Solution and mounted on gelatine-coated slides using fluorescence mounting medium (DAKO). AAV8 spread in constitutive *Adamtsl3* knock-out mice (RFP/RFP-Cre) and inducible *Adamtsl3* and *DCC* knock-out mice (stained for Cre protein) were assessed using a 10× objective. Animals exhibiting insufficient virus spread were excluded from further morphological analysis. z stack images (4 optical sections, 0.5μm step size) were recorded of all sections using near super-resolution Airy scan microscopy (CLSM 800 Airyscan, Carl Zeiss). Images were taken using a 40× objective with a numerical aperture of 1.4, and pixel size of 112 nm^2. 4–5 juxtaposed images of the CA1 *Stratum pyramidal* or *Stratum radiatum* were taken. To reduce variability, multiple images were captured from 3 sections per mouse and a minimum of 3 mice were analyzed per experimental group and puncta density values and co-localized puncta values were averaged from these sections. All imaging parameters were kept constant between knock-out and control animals. A custom Python script using the ImageJ image-processing framework was used for puncta analysis. The script can be used as a plugin and is openly available on a GitHub repository (https://github.com/dcolam/Cluster-Analysis-Plugin). The plugin provides a rapid and unbiased puncta quantification tool in image analysis, as it allows the usage of both default and self-defined parameters. In brief, puncta identification is followed by the detection of their spatial overlap (co-localization). For co-localization analysis, selections of individual puncta were enlarged by 0.1μm to prevent possible edge exclusions and co-localization was defined when over 50% puncta overlapped. Representative example images were processed using ImageJ. Statistical tests were performed using Prism software (GraphPad) using a minimum of 3 mice per group.

Immunoprecipitation and WB

Immunoprecipitation and WB protocols were performed using whole cell lysate from HEK293T cells or P90-P120 old mouse lung, liver, spleen, heart, kidney and brain in EBC lysis buffer (50 mM Tris, pH 7.6, 150 mM NaCl, 1% Triton X-100 containing CompleteMini Protease Inhibitor from Roche and phosphatase inhibitor mixture 1 and 3 from Sigma Aldrich). For immunoprecipitation, 2 μg of anti-Adamtsl3 antibody were used to precipitate GFP-tagged Adamtsl3 in serum-free media of transfected HEK293T cells for 90 min at 4°C on a rotor. Complexes were then collected by incubating with 25 μL of Pierce Protein A/G Ultralink Resin (Thermo Fisher Scientific, Cat.# 53132) for 45 min at 4°C on a rotor. Complexes were centrifuged and washed 3x in ice-cold EBC buffer to remove nonspecific interactions. HEK293T cell lysate expressing pCMV-myc-DCC was added to the resin for an additional 90 min incubation at 4°C on a rotor. Complexes were centrifuged and washed 3x in ice-cold EBC buffer to remove nonspecific interactions, followed by denaturation in 2 x SDS loading buffer at 90°C for 5 min. The immunoprecipitated complexes were analyzed using WB.

WB analysis of mouse lung, liver, spleen, heart, kidney and brain were performed following homogenization and 1h incubation on ice in EBC lysis buffer. Lysates were centrifuged at 20,000 RPM for 30 min at 4°C and supernatants were stored at −80°C. Proteins were analyzed using WB. Samples were run on Tris-glycine polyacrylamide gels and proteins were transferred to PVDF membranes. Primary antibodies (key resources table) were incubated in Tris-buffered saline with 0.05% Tween 20 (TBST), including 5% WesternBlocking solution (Roche) overnight at 4°C. Membranes were washed 5 × 5 min in TBST. HRP-coupled donkey secondary antibodies (1:30,000) and fluorescent-coupled donkey secondary antibodies (1:20,000) were incubated for 30 min at room temperature, and membranes were washed again 5 × 5 min in TBST. Fluorescent signals were captured using the Odyssey CLx Imager. SuperSignal West PICO Chemiluminescent substrate (Thermo Fisher Scientific) was applied to visualize HRP labeled antibodies and developed using the Luminescent Image Analyzer LAS-1000 plus & Intelligent Dark Box IItbox2 (Fujifilm). Images were analyzed using ImageJ and statistical tests were performed using Prism software (GraphPad) using a minimum of 3 mice. WB membrane stripping for re-staining was performed using a mild stripping protocol as described by the manufacturer (Abcam): membranes were incubated twice for 5–10 min with mild stripping buffer (200mM glycine, 20mM SDS, 0.01% Tween 20, pH 2.2) followed by 2 × 10 min incubation with PBS and 2 × 5 min incubations with TBST. The efficiency of stripping was determined by incubating with chemiluminescent substrate. After stripping the membranes were rinsed and incubated again with primary antibody.

In situ proximity ligation assay (in situ PLA)

In situ PLA was performed using the Duolink II kit (Sigma Aldrich) according to the instructions of the manufacturer. Briefly, primary hippocampal neurons seeded on coverslips were washed for 5 min with PBS and then fixed with 4% PFA for 30 min at room

temperature. Then, the coverslips were rinsed in PBS for 5 min and permeabilized for 15 min with 0.2% Triton X-100/PBS. After rinsing the coverslips in PBS, they were incubated with homemade Adamtsl3 antibody (1:50) and myc-tag antibody (1:50) and kept in a humidity chamber overnight at 4°C. Subsequently, the coverslips were washed 4 × 5 min with PBS and incubated for 20–30 min at room temperature with PLA probes (prepared by diluting anti-mouse MINUS and anti-rabbit PLUS, Duolink II, 1:5 in 5% BSA/PBS). Afterward, 40 μL of the PLA probe solution was pipetted on top of each coverslip and incubated in a humidity chamber for 1 h at 37°C. The coverslips were then washed twice for 5 min in PBS and incubated for 1 h at 37°C with ligation solution. Subsequently, the cells were washed twice in Duolink II Wash Buffer A and incubated with the amplification solution at 37°C for 100 min. Finally, the coverslips were washed twice for 10 min with Duolink II Wash Buffer B in the dark and mounted onto microscope slides using fluorescent mounting medium (DAKO).

Synaptoneurosomes preparation

Synaptoneurosomes were prepared from mouse forebrain.[71] Briefly, brains were isolated, washed and homogenized in ice-cold sucrose buffer (320 mM sucrose, 5 mM HEPES, pH 7.4) using a Teflon-glass tissue grinder. The homogenate was centrifuged at 1000g for 10 min 2mL of the supernatant was loaded over discontinuous Percoll gradients (3, 10, and 23% Percoll in sucrose buffer), followed by centrifugation at 31,000g for 5 min. Interface fractions between 3 and 10% and 10 and 23% were collected and further centrifuged at 20,000g to pellet synaptoneurosomes. All centrifugation steps were performed at 4°C. All solutions were supplemented with a complete protease inhibitor cocktail (Roche), 0.05 mM dithiothreitol (DTT), 0.1 mM phenylmethylsulfonyl fluoride, and 20 U/10 mL RNaseOUT (Invitrogen).

Slice preparation and electrophysiological recordings

Mice were anesthetized by isoflurane, decapitated and their brains were rapidly transferred to ice-cold dissecting artificial cerebral spinal fluid (ACSF) containing (in mM): 75 Sucrose, 87 NaCl, 2.5 KCl, 1.25 NaH2PO4, 7 MgCl2, 0.5 CaCl2, 25 NaHCO3 and 25 D-glucose, saturated with 95% O_2 and 5% CO_2. Coronal sections (270μm thick) were cut in the dissecting artificial cerebral spinal fluid (ACSF) using a vibratome (VT 1200S), Leica slicer, and then transferred to normal ACSF containing (in mM): 115 NaCl, 3.5 KCl, 1.2 NaH_2PO_4, 1.3 $MgCl_2$, 2 $CaCl_2$, 25 $NaHCO_3$, and 25 D-glucose and aerated with 95% O_2 and 5% CO_2. Slices were kept at room temperature and recovered in ACSF for 30 min before recording. Slices were then placed in the recording chamber of an upright microscope (Axioscope 2 FS, Zeiss) and superfused with 32°C oxygenated (95% O2 and 5% CO2) ACSF at a 2 mL/min rate. The microscope was equipped with immersion differential interference contrast (DIA) and the following objectives was used to visualize neurons in the hippocampal CA1 *Stratum pyramidale* region. (10X/0.3, Olympus and 40X/0.8, Zeiss). A CMOS camera (optiMOS, QImaging) was attached to the scope to visualize the slice and cells through a computer screen.

Voltage clamp experiments were performed on CA1 pyramidal neurons using borosilicate patch pipettes (1.5 OD X 0.86 ID X 75 L mm, Harvard Apparatus at a resistance of 3–4 MΩ) filled with a solution containing (in mM): 130 $CsMeSO_3$, 5 CsCl, 5 NaCl, 2 $MgCl_2$, 0.1 EGTA, 10 HEPES, 0.05 $CaCl_2$, 2 Na2-ATP, 0.4 Na_3-GTP (pH 7.3, 280–290 mOsm/kg). Each CA1 pyramidal neuron was voltage-clamped at −70 mV and 0 mV to record miniature inhibitory postsynaptic currents (mIPSCs). mIPSCs were recorded in the gap-free mode for 3 min, and by adding to the recording solution 0.5 μM TTX, to block voltage-gated Na^+ channels. Data were acquired using an Axopatch 200B amplifier controlled by pClamp software (v10.7.0.3, Molecular Devices 2016), filtered at 2.4 kHz and sampled at 10 kHz (Digidata 1440A, Molecular Device). Series resistance (range 15–20 MΩ) was monitored at regular intervals throughout the recording and presented minimal variations (≤20%) in the analyzed cells. Data are reported without corrections for liquid junction potentials. mIPSCs inter-event interval and amplitude were analyzed offline using Minianalysis software (Synaptosoft, Decatur, GA).

iLTP and cLTP in primary neuron culture

As described above, primary hippocampal neuron cultures were prepared from P0-1 *Adamtsl3*$^{flox/flox}$ pups. At 4DIV, cultures were infected with AAV8-hSyn1-RFP-Cre (AAV8-hSyn1-RFP control) to delete the *Adamtsl3* gene. Inhibitory LTP (iLTP) was induced at 14DIV by adding 20 μM NMDA and 10 μM CNQX for 2 min at room temperature. Afterward, the media was replaced with conditioned media and neurons were returned to the incubator for 60 min before fixation and immunocytochemistry.

Chemical long-term potentiation (cLTP) was induced at 14DIV in cultured hippocampal neurons from *Adamtsl3*$^{flox/flox}$ mice.[72,73] Before stimulation, neurons were incubated at room temperature for 20 min in a control solution (125 mM NaCl, 2.5 mM KCl, 1 mM MgCl2, 2 mM CaCl2, 33 mM D-glucose, 5 mM HEPES, 20 μM D-APV, 3 μM strychnine, 20 μM bicuculline and 0.5 μM TTX; pH 7.4). cLTP was induced for 10 min at room temperature using a control solution lacking Mg^{2+}, TTX, and D-APV but glycine (200 μM). After cLTP regular control solution was added back to neurons and returned to the incubator for 40 min before fixation and immunocytochemistry.

Stereotactic surgery

30 min before the surgical procedure, mice received 0.1 mg/kg buprenorphine (s.c. injection) and 10 mL/kg 25% (w/v) D-Mannitol i.p. to improve viral absorbance. Mice were anesthetized via inhaled isoflurane (initially 5% for induction, then 2% via mask) and placed on a warming pad to prevent a drop in body temperature. Eyes were protected via vitamin A ointment. After fixing the mouse head in a stable position in a stereotaxic frame, local anesthesia and anti-inflammatory agent were applied using s.c. injection (26 G needle, inject a small volume) of lidocaine & bupivacaine (both diluted to 0.5%; 5 mg/ml, inject 20 μL/25 g b.w.) at the surgical site 5 min before

surgery. Then, an incision was made along the midline to expose the skull. After cleaning the skull, a hole was drilled in the injection site. The virus was subsequently injected (10^{e12} infectious units AAV8-hSyn1-shRNA-eGFP-scramble or AAV8-hSyn1-shRNA-eGFP-NTN1, 300-800nL saline, artificial cerebrospinal fluid) using a stereotaxically positioned motorized microinjector (Drummond Scientific Company, Nanoject II, 50 nL/s, 0.1 mm tip diameter). The coordinates of the injection site for the hippocampus used were: dorsal hippocampus, AP = −1.9mm, DV = −1.0mm, LM = +/−1.6 from bregma. Following injection, the skin was sutured (Dafilon 45cm) and mice were placed in a recovery cage equipped with a heating pad and lined with tissue. Once the mice recovered fully, they received 400μL of pre-warmed 5% glucose solution s.c. before returning to the home cage. Buprenorphine (Temgesic 0.1 mg/kg) was given after the surgical procedure for 3 days.

Object displacement test and novel object recognition test

Mice were trained and tested using the object displacement test (ODT) as a non-invasive measure of hippocampal-dependent spatial memory. We employed the novel object recognition (NORT) test to assess for recognition memory. All experiments are performed at the same time of day, 1 h after normal light onset to control for circadian rhythms. To minimize potential disruptions by human handling, the experimenter repeatedly and over the course of 2 months carefully handled the mice every week starting after weaning (P20-P25). Behavior analysis was conducted between P90-P105. On Day 1, mice were habituated to the empty square testing chamber (50 cm × 36 cm, 26 cm-high walls). On Day 2, mice were presented with two identical objects placed horizontally next to each in the testing chamber. For spatial orientation, one wall was marked with a centered, vertical line reaching from top to bottom. 24 h later, one of the objects was moved to a novel location (ODT) or replaced with a novel object at the same location (NORT) in the testing chamber. An overhead camera recorded the mice for 10 min throughout training and testing. Objects and the test chamber were cleaned with 70% ethanol between trials to remove olfactory cues. An experimenter blind to the genotypes measured exploration time. Exploration times were calculated as the total time the animal investigated each object (sniffing the object). The discrimination index was calculated as the time spent exploring the displaced/novel object divided by the total time spent exploring both objects.

QUANTIFICATION AND STATISTICAL ANALYSIS

Expect for electrophysiological data, statistical analyses were performed using one-way ANOVA or unpaired t test where appropriate and presented as mean ± s.d. The mIPSC/mEPSC data are presented as mean ± S.E.M. and the two groups were tested for statistical significance using the Mann Whitney U-non parametric test or unpaired t test. Statistical significance was determined with $p \leq 0.05$. Data were analyzed and processed using Fiji ImageJ and GraphPad Prism 6 software. The custom Python script using the ImageJ image-processing framework can be used as a plugin and is openly available on a GitHub repository: https://github.com/PDKlab/Exocytose-EventsDetection. Plotted data were then formatted in Affinity Designer 1.8.5.703.